# Orientational epitaxy and lateral structure of the hexagonally reconstructed Pt(001) and Au(001) surfaces

D. L. Abernathy and S. G. J. Mochrie
*Research Laboratory of Electronics and Department of Physics, Massachusetts Institute of Technology, Cambridge, Massachusetts 02139-4307*

D. M. Zehner
*Solid State Division, Oak Ridge National Laboratory, Oak Ridge, Tennessee 37831-6057*

G. Grübel* and Doon Gibbs
*Department of Physics, Brookhaven National Laboratory, Upton, New York 11973-5000*
(Received 13 May 1991; revised manuscript received 4 November 1991)

We present results of synchrotron-x-ray-scattering studies of the orientational epitaxy exhibited by clean, hexagonally reconstructed Pt(001) and Au(001) surfaces. For the Pt(001) surface, a high-symmetry direction of the hexagonal overlayer is aligned with a high-symmetry direction of the bulk between 1820 and 1685 K. Between 1685 and ~1580 K, the relative rotation angle varies continuously from 0° to 0.75° with a one-half-power-law dependence on the reduced temperature. At ~1580 K, domains with a rotation angle of 0.8° appear discontinuously, in coexistence with those with a rotation angle of 0.75°. The two rotation angles reach ~0.9° and ~0.75° for the continuously and discontinuously rotated components, respectively, at 300 K. At all temperatures, the overlayer is incommensurate along both directions of the surface, with weakly temperature-dependent incommensurabilities. The areal density of the Pt(001) overlayer is compressed by ~8% with respect to the hexagonal (111) planes in the bulk. In addition, the extent of translational order within the surface layer decreases with decreasing temperature. The Au(001) surface exhibits a strongly discontinuous rotational transformation at ~980 K and there is coexistence between rotated and unrotated domains, in agreement with previous measurements. Rotated domains appear at a rotation angle of ~0.8° and their number grows with decreasing temperature at the expense of unrotated domains. Our measurements reveal the existence of additional favored rotation angles: one of 0.9° and one that varies smoothly from 0° to 0.5°. The relative domain populations depend on temperature. A mean-field theory of rotational transformations, which accounts for the continuous rotational behavior of the Pt(001) surface, is presented, and it is shown that there are no corrections to mean-field behavior from fluctuations for a rotational transformation.

## I. INTRODUCTION

A basic issue for the growth of one crystal on another concerns their relative orientation: How are the high-symmetry directions of the two lattices aligned? Present understanding of this question has been guided by the calculations of Novaco and McTague,[1] who explicitly considered hexagonal, incommensurate overlayers of the rare gases (Ne, Ar, Kr, and Xe) adsorbed on a graphite basal plane substrate. They showed that, even though there is no translational registry between an incommensurate overlayer and a substrate, there exists a preferred orientational relationship. This is called orientational epitaxy. Specific model calculations reveal that the high-symmetry directions of an incommensurate overlayer may be rotated away from the high-symmetry directions of the substrate and that the relative rotation angle is determined by the incommensurability of the overlayer and by the frequencies of its lattice vibrations (phonon dispersion relations). In many instances, the predictions of Novaco and McTague qualitatively, and often quantitatively, describe the orientational epitaxy of an adsorbed layer, most notably for rare gases on graphite[2–6] and for alkali metals on transition-metal substrates.[7,8] Other systems for which the rotational epitaxy has been characterized include layers of the alkali metals intercalated into graphite,[9,10] *in situ* monolayers of Pb electrochemically deposited on Ag(111) and Au(111) electrodes,[11] small three-dimensional crystallites of Pb deposited on Si(111) and Ge(111) substrates,[12,13] and the Au(001) surface under electrochemical conditions.[14]

Both the Pt(001) (Refs. 15–21) and the Au(001) (Ref. 22) surfaces in vacuum reconstruct to form close-packed hexagonal monolayers (the overlayer) on top of bulk planes of square symmetry (the substrate). In each case, the overlayer and the substrate are incommensurate. In this paper, we present x-ray-diffraction measurements of the lateral structure of the Pt(001) overlayer between 300 and 1820 K, including, in particular, its orientational epitaxy. We also present measurements concerning the orientational behavior of the reconstructed Au(001) surface, which extend and clarify our earlier results for this surface.[22] A complete account of our procedures, data, and analysis is given here; a summary appears elsewhere.[23]

An important result of the present study is that the phase behavior of the Pt(001) surface mirrors that of the Au(001) surface.[22] In both cases, we have identified three

 

distinct structural phases. They are, in order of decreasing temperature, disordered, aligned-hexagonal, and rotated-hexagonal. Furthermore, when considered on a temperature scale normalized by the bulk melting temperature ($T_m = 2045$ K for Pt and 1337 K for Au), the transformation temperatures between the different phases of the Pt(001) surface are strikingly similar to those of the Au(001) surface. For temperatures in the range $T_m > T > 0.89T_m$, the Pt(001) surface is disordered and there is no scattering at wave vectors associated with the reconstruction.[24] The Au(001) surface is disordered for $T_m > T > 0.88T_m$.[22] At a temperature of $0.89T_m$, the Pt(001) surface undergoes a phase transformation into a hexagonal phase. Figure 1(a) schematically illustrates the surface structure and Fig. 1(b) shows the *HK* plane of the corresponding reciprocal space. For clarity, only regions

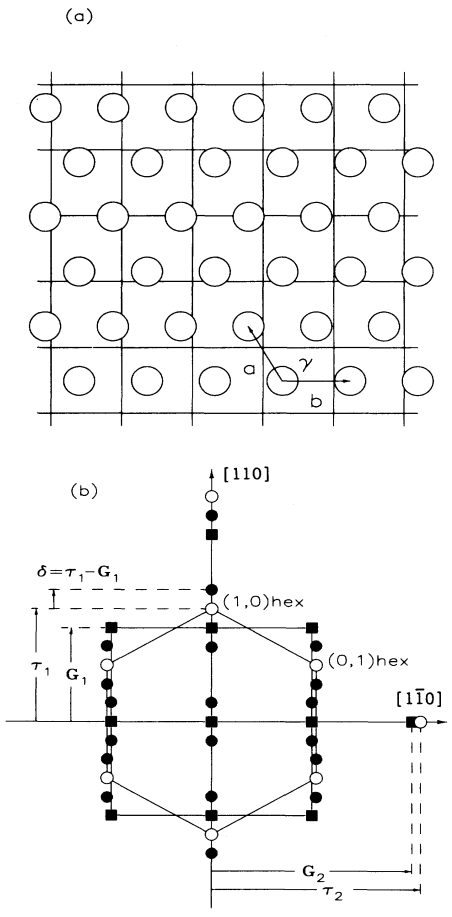


FIG. 1. Aligned-hexagonal phase of the Pt(001) surface. (a) Real space schematic of the hexagonal overlayer on the square substrate. Vertical lines indicate the bulk [110] direction and horizontal lines the [1$\bar{1}$0] direction. (b) *HK* plane of reciprocal space. Scattering from the substrate (solid squares), hexagonal surface layer (open circles), and satellites (dark circles) form rods extending normal to the surfaced. Observed peaks as well as symmetry equivalents are shown. In our experiments, we have observed two equivalent orientations of surface reconstruction domains related by a rotation of 90° about the surface normal. For clarity, Figs. 1 and 2 display the wave vectors associated with only one of these orientations.

of the surface with a principle hexagonal wave vector oriented along the [110] direction are shown, although the other possible orientation of the surface reconstruction is also observed. Each symbol in Fig. 1(b) represents a rod of scattering which extends in the direction perpendicular to the surface ($L$ direction). Immediately below the transformation, the overlayer lattice is aligned with the substrate lattice in the sense that the (1,1,0) cubic substrate wave vector ($\mathbf{G}_1$) and the (1,0) hexagonal overlayer wave vector ($\tau_1$) are parallel. It follows that the two lattices share a high-symmetry direction. In addition to the rods of scattering from the substrate [truncation rods, shown as solid squares in Fig. 1(b)] and from the hexagonal overlayer [overlayer rods, shown as open circles in Fig. 1(b)], there are also satellite rods [solid circles in Fig. 1(b)], displaced from hexagonal or substrate wave vectors by a wave vector ($\delta$), which is equal to the difference between $\tau_1$ and $\mathbf{G}_1$. The presence of such satellites suggests that the overlayer and the substrate lattices are both subject to a distortion, which is characterized by the wave vector $\delta$. The Au(001) surface likewise transforms into an aligned-hexagonal phase at $0.88T_m$. For the Au(001) surface, our previous measurements have shown that the distortion is a surface corrugation, which penetrates with diminished amplitude several layers into the bulk.[22] (In this paper we refer to a structural modulation in which the atomic displacements are perpendicular to the surface as a corrugation.)

On cooling, there is a range of temperature in which the surface and substrate lattices remain aligned. However, at still lower temperatures, the overlayer is rotated with respect to the substrate. Figure 2 illustrates the *HK* plane of reciprocal space for the rotated-hexagonal phase of the Pt(001) surface. In this figure, filled squares correspond to truncation rods, open circles correspond to overlayer rods, and solid circles correspond to satellite rods. The appearance of rotated domains of the hexagonal reconstruction is signaled in the diffraction pattern by the appearance of rods of scattering, which are split at a common angle away from the locations of each of the original, aligned overlayer rods. Thus there are domains with both positive and negative senses of rotation. The angular displacement about the origin of reciprocal space is equal to the rotation angle of the corresponding surface domain. As can be seen from Fig. 2, $\tau_1$ and $\mathbf{G}_1$ are no longer parallel in the rotated-hexagonal phase.

In the case of the Au(001) surface, our earlier measurements[22] showed that the alignment of some fraction of the overlayer changes discontinuously at $0.74T_m$. Rotated domains were observed with a fixed rotation angle of 0.8° in coexistence with unrotated domains. The population of rotated domains was found to grow with decreasing temperature and the population of unrotated domains to decrease correspondingly. Measurements presented in this paper reveal additional details, including the existence of domains with a rotation angle of 0.9° and the existence of domains for which the rotation angle appears to vary continuously with temperature from 0° to 0.5°. The population of each of the differently oriented domains depends on temperature and on cooling rate. Nevertheless, the transformation is reversible, and the

same rotation angles are reproduced on different cycles of the temperature. The incommensurability along the [110] direction, defined to be $\tau_1/G_1-1$, varies from $0.206\pm0.001$ at $0.88T_m$ to $0.205\pm0.001$ at 300 K for the Au(001) surface. ($\tau_1$ and $G_1$ are the magnitudes of $\tau_1$ and $\mathbf{G}_1$, respectively.)

The rotational transformation of the Pt(001) surface, which occurs at a critical temperature of $T_c=0.82T_m=1685$ K, is continuous. Close to the transformation, the rotation angle ($\theta$) varies smoothly, with a one-half-power-law dependence on the reduced temperature $[(T_c-T)/T_c]$. There is no unrotated component below $T_c$; however, at about 1580 K, there is a second, discontinuous rotational transformation, which leads to coexistence among domains with slightly different rotation angles. Below 1580 K, the observed rotation angles evolve slightly with further decrease of the temperature, reaching 0.75° and 0.9° at 300 K for the discontinuously and continuously rotated components, respectively. It is important to emphasize that for the Pt(001) surface the overlayer lattice constants are only weakly temperature dependent between 300 K and the disordering transition; the incommensurability along the [110] direction varies from $0.2022\pm0.0003$ at 1820 K to $0.204\pm0.001$ at 300 K.

In its simplest form, the theory of Novaco and McTague[1] predicts that the rotation angle is approximately linearly related to the incommensurability. In particular, the rotation angle predicted for an incommensurability of $\sim0.2$ is $\sim7°$, which is roughly a factor of 10 larger than any of the observed rotation angles shown by the Pt(001) or Au(001) overlayers. It seems clear, therefore, that our results concerning the temperature dependence of the observed rotation angles and incommensurabilities, the coexistence of domains with different rotation angles, and the magnitudes of the observed rotation angles stand outside a straightforward application of Ref. 1, or related theories.[25,26] We believe that the discrepancies originate from several assumptions. First, the theory of Novaco and McTague assumes that pair potentials can be used to describe the interactions among the surface and substrate atoms. Such an approach fails to provide an adequate description of metallic binding or of metal surface structures.[27] Second, Novaco and McTague take the substrate to be rigid and the atomic displacements to be small. In contrast, our results show that there is a significant substrate corrugation at the Au(001) surface,[22] and we infer a similar corrugation at the Pt(001) surface. Third, it is assumed in their theory that the temperature is zero.

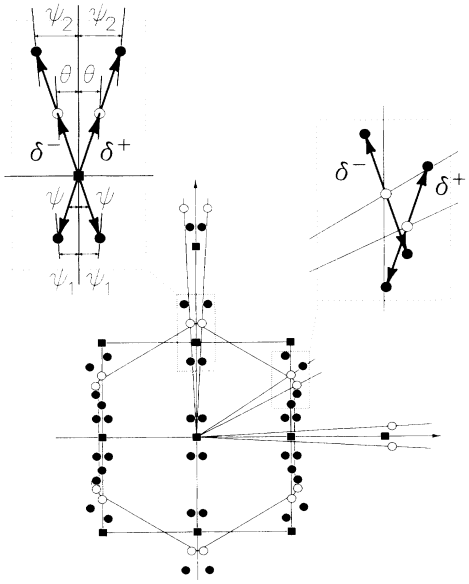


FIG. 2. Rotated hexagonal phase of the Pt(001) surface. Solid squares indicate the positions of the truncation rods and open circles indicate the positions of the overlayer rods. The positions of observed satellite rods and their symmetry equivalent are shown as solid circles. From our measurements in the aligned-hexagonal phase, and from the known rotation angle, we infer the existence of satellite rods at the positions indicated by the shaded circles. In general, we expect there to be a satellite associated with each hexagonal rod and each truncation rod. However, in this figure we have indicated only those directly observed in the rotated- or aligned-hexagonal phases during the course of our experiment.

The magnitudes of the observed rotation angles and the coexistence among domains with differing rotation angles remain unexplained. However, motivated by the observation that the rotation angle follows a one-half-power law versus reduced temperature in the case of the Pt(001) surface, we have developed a simple mean-field theory which accounts for the variation of the rotation angle with temperature near $T_c$: $\theta=A[(T_c-T)/T_c]^{1/2}$. Moreover, we show that, for a rotational transformation, there are no corrections to the results of mean-field theory from fluctuations. It seems possible, therefore, that continuous, temperature-driven, rotational transformations may, in general, exhibit mean-field behavior. (We emphasize that such transformations are distinct from continuous, rotational transformations which occur by virtue of a varying incommensurability.[25,26]) For certain values of the parameters, our theory predicts a discontinuous variation of the rotation angle with temperature (first-order phase transformation), which is suggestive of the rotational behavior of the hexagonally reconstructed Au(001) surface.

The present study also demonstrates that the nearest-neighbor separation within the hexagonal overlayer of the Pt(001) surface is about 4% smaller than the bulk nearest-neighbor separation. This result conforms to the pattern set by the hexagonal reconstruction of the Au(001) surface[22] and by the high-temperature reconstruction of the Au(111) surface,[28] each of which shows a compressed hexagonal layer, in which the nearest-neighbor distance is $\sim4\%$ contracted relative to the bulk nearest-neighbor distance. Recent calculations indicate that atoms at metal surfaces favor a smaller nearest-neighbor separation than atoms in the crystal interior, so that unreconstructed metal surfaces are under a tensile stress.[29–32] It has further been suggested[29] that the relief of surface stress gives rise to the reconstructions of the Au(001), Au(111), and Pt(001) surfaces. The accumulated results for all three surfaces tend to support this assertion.

Finally, our experiments show that the extent of

translational order decreases with decreasing temperature within the rotated-hexagonal phase of the Pt(001) surface [as also occurs for the Au(001) surface[22]]. It is possible that this unusual behavior will be understood within the framework of a recent proposal that high-symmetry surfaces, which can reconstruct into one of several, rotationally equivalent structures, are unstable to the formation of domains.[33]

The format of this paper is as follows: In Sec. II, we detail our experimental procedures. In Sec. III, we present data obtained for the Pt(001) surface: Sec. III A describes the aligned-hexagonal phase, Sec. III B describes the rotated-hexagonal phase, and Sec. III C describes the rotational phase transformation between these two structures. In Sec. IV, we report measurements of the orientational epitaxy of the hexagonally reconstructed Au(001) surface and compare the orientational behavior of the Au(001) surface to that of the Pt(001) surface. We present a mean-field theory of rotational transformations in Sec. V. In Sec. VI, we summarize and conclude. The effects of different cooling rates on the structure of the hexagonal overlayers are described in the Appendix.

## II. EXPERIMENTAL PROCEDURES

The experiments reported in this paper were performed on Beamline X22C at the National Synchrotron Light Source, using an ultra-high-vacuum (UHV) apparatus specifically designed for x-ray-scattering studies of surfaces. Both the beamline[34] and the apparatus[35] have been described in detail elsewhere.

A (001)-oriented boule of Pt was cut to produce a disk 2 mm thick and 8 mm in diameter, which was then mechanically polished to within 0.2° of the crystallographic [001] direction. The mosaic width was about 0.01° full width at half maximum (FWHM). The sample was supported using two tantalum wires threaded through slots cut into the sides of the disk. After insertion into the UHV apparatus, the Pt(001) surface was prepared by $Ar^+$-ion bombardment (1 kV and 7 $\mu$A for 60 min), followed by heating at 1200 K in an atmosphere of $10^{-7}$ Torr of $O_2$ for 4–6 h. After repeated cycles of this procedure, the surface was clean as determined by Auger electron spectra (AES) obtained using a single-pass cylindrical mirror analyzer. In addition, the observed diffraction patterns remained reproducible at high temperatures for extended periods. [Prior to extended heating in $O_2$, significant amounts of C on the surface were detected by means of AES, especially following periods in which the sample was held at elevated temperatures ($\sim$1800 K).] Sample heating was achieved by accelerating electrons evaporated from a tungsten filament through a potential of 1 kV onto the back of the sample. By controlling the filament current, it was possible to control the sample temperature between 300 and 2000 K. The chamber pressure was maintained at $<10^{-9}$ Torr throughout the experiment. The sample temperature was monitored with a *W* $Re_{0.05}$-*W* $Re_{0.26}$ thermocouple and, more reliably, by direct measurement of the Pt lattice constant, using the relationship given in Ref. 36. The cubic lattice constant of Pt at 300 K was used to calibrate the x-ray wave number, which was typically 4.08 $Å^{-1}$. On different temperature cycles, the measured value of the rotational transformation temperature was found to vary by less than $\pm$10 K, which we take to be the error. Our best estimate is that $T_c = 1685 \pm 10$ K. Within a given cycle of the temperature, we could determine temperature differences to $\pm$1 K. Where necessary, in Sec. III, we have adjusted the temperature scale to locate the transformation temperature at $T_c = 1685$ K.

The Au(001) sample used in the present measurements was the same one studied in Ref. 22. It was a disk 2 mm thick and 10 mm in diameter with a mosaic width of 0.03° FWHM. Our surface preparation procedures closely followed those described above for the Pt(001) surface. In this instance, however, no $O_2$ treatment was performed.

The x-ray-scattering measurements reported in the present paper were obtained with the incident and scattered x rays at a glancing angle to the surface, so that the wave-vector transfer (**Q**) is essentially confined to the *HK* plane of reciprocal space. A pair of near-perfect Ge(111) crystals of angular acceptance $\sim$0.007° FWHM was employed as a monochromator. Similarly, a near-perfect Ge(111) crystal was employed as an analyzer crystal before the detector, defining the angular acceptance within the scattering plane to be $\sim$0.007° FWHM. Slits defined the acceptance perpendicular to the scattering plane (out of plane). This configuration matches the diffuse direction of the x-ray-scattering cross section of a two-dimensional structure to the relatively large out-of-plane acceptance, while the resolution within the scattering plane (*HK* plane) is determined by the collimation of the incident x rays and by the analyzer crystal. (The vertical opening angle of the synchrotron is 0.014° FWHM.) The use of a glancing incidence and glancing exit geometry and the accompanying fine reciprocal space resolution allows the lattice constants and orientation of the overlayer to be determined accurately.

## III. PLATINUM (001) SURFACE—RESULTS AND DISCUSSION

### A. Aligned-hexagonal phase

Between 1820 and 1685 K, the Pt(001) surface exhibits a hexagonal reconstruction for which the (1,0) principal hexagonal wave vector ($\tau_1$) is aligned with the (1,1,0) cubic wave vector ($\mathbf{G}_1$). The corresponding diffraction pattern is illustrated in Fig. 1(b). Figure 3 shows the results of several radial scans along the cubic [110] direction, obtained at 1810 K. The (1,0) hexagonal rod appears at $\zeta = 1.2022$ [Fig. 3(c)] and the (1,1,0) cubic substrate rod (truncation rod) appears at $\zeta = 1.000$ [Fig. 3(b)]. For these scans, the wave-vector transfer is related to $\zeta$ via $\mathbf{Q} = (2\pi/c)(\zeta, \zeta, 0.06)$, where $c$ is the cubic lattice constant of Pt. (At 1810 K, $c = 3.991$ Å.) At the (1,0) hexagonal rod, the peak count rate was approximately 60,000 per second for an electron current in the storage ring of 150 mA. These data [Figs. 3(b) and 3(c)] demonstrate that there is not a simple rational relationship be-

tween the magnitudes of $\tau_1$ and $\mathbf{G}_1$ and suggest that the hexagonal overlayer and the substrate are incommensurate along the cubic [110] direction. It is convenient to define their difference wave vector as $\delta$. We further define the incommensurability along the [110] direction to be $\tau_1/G_1-1$, so that, at 1810 K, the incommensurability is 0.2022 along the [110] direction. Two additional satellite peaks appear in Fig. 3, with peak intensities down by a factor of more than 1000 compared to the hexagonal rod. There is a peak at $\zeta=1.4044$ [Fig. 3(d)], which is displaced from $\tau_1$ by exactly $\delta$, and a peak at $\zeta=0.2022$ [Fig. 3(a)], which is displaced from the origin of reciprocal space by exactly $\delta$. We also observed a satellite displaced from $\mathbf{G}_1$ by $-\delta$ (not shown). However, satellites at $\mathbf{G}_1-2\delta$ or $\tau_1+2\delta$ were not observed.

Figure 4 shows the results of radial scans along the cubic $[1\bar{1}0]$ direction, across the substrate rod through $(2,-2,0)$ ($\mathbf{G}_2$), and also through the hexagonal $(-1,2)$ rod ($\tau_2$) at $\zeta=2.0813$. For these scans the wave-vector transfer is related to $\zeta$ via $\mathbf{Q}=(2\pi/c)(\zeta,-\zeta,0.06)$. These scans suggest that the overlayer is also incommensurate with the substrate along the cubic $[1\bar{1}0]$ direction, with an incommensurability of $\tau_2/G_2-1=0.0406$. No satellites were observed in this direction, indicating that the dominant modulation in the plane of the surface is along the [110] direction. The observed positions of the overlayer rods, of the truncation rods, and of the satellite rods, which are summarized in Fig. 1(b) together with their symmetry equivalents, allow us to estimate that the error in our determination of the incommensurabilities is less than 0.0003 at 1810 K.

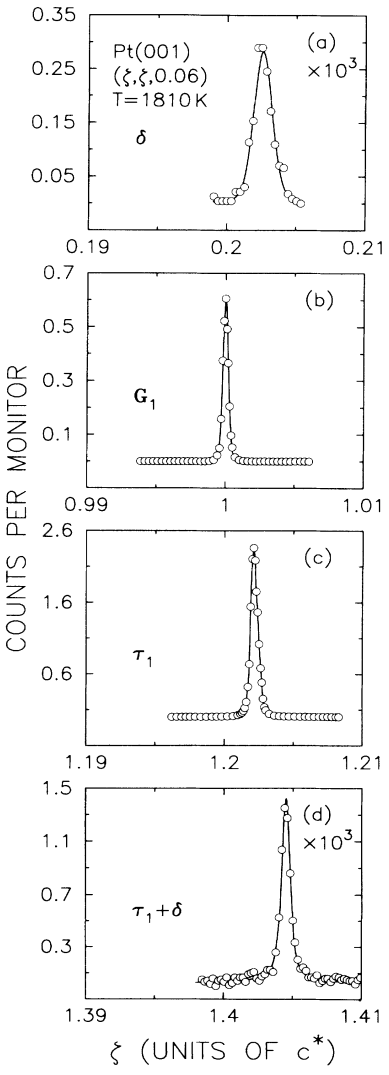


FIG. 3. Radial scans along the [110] direction for the aligned-hexagonal phase of the Pt(001) surface. These data were collected with $L=0.06$ and in-plane wave-vector transfers of (a) $\delta$, (b) $\mathbf{G}_1$, (c) $\tau_1$, and (d) $\tau_1+\delta$. The solid lines are guides to the eye.

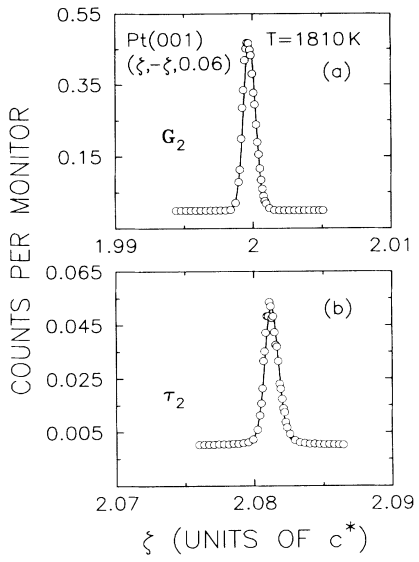


FIG. 4. Radial scans along the $[1\bar{1}0]$ direction for the Pt(001) surface in the aligned hexagonal phase. These data were collected with $L=0.06$ and in-plane wave-vector transfers of (a) $\mathbf{G}_2$ and (b) $\tau_2$. The solid lines are guides to the eye.

From measurements of the incommensurabilities along the [110] and $[1\bar{1}0]$ directions, it is possible to calculate the average lattice constants of the overlayer. They are as follows: $a=2.711\pm0.0001$ Å, $b=2.712\pm0.001$ Å, and $\gamma=120.02°\pm0.04°$ at 1810 K. At this temperature, therefore the structure of the Pt(001) overlayer is accurately hexagonal. It is, however, contracted relative to the hexagonal (111) planes in the crystal interior, where the Pt nearest-neighbor distance is 2.822 Å at 1810 K. Specifically, the reconstructed hexagonal overlayer is contracted by $(3.93\pm0.03)\%$ along the [110] direction and by $(3.90\pm0.03)\%$ along the $[1\bar{1}0]$ direction. These results are strikingly similar to our earlier results for the Au(001) surface, where the hexagonal reconstruction is contracted by 4.3% in the [110] direction and by 4.2% in the $[1\bar{1}0]$ direction, relative to the (111) places of bulk Au.[22] In this regard, it is noteworthy that the areal density of the reconstructed Au(111) surface at high temperatures, which also shows a hexagonally reconstructed layer, is similarly increased by about 8% relative to the (111)

planes of bulk Au.[28] Recent calculations by Needs and Mansfield,[29,30] by Dodson,[31] and by Takeuchi, Chan, and Ho[32] indicate that atoms at metal surfaces may have a smaller natural nearest-neighbor separation than in the crystal interior. According to this view, unreconstructed metal surfaces experience a tensile stress. It has been proposed[30] that the relief of surface stress gives rise to the hexagonal reconstructions of the Au(111), Au(001), and Pt(001) surfaces. Our determination that the area per atom of the hexagonally reconstructed Pt(001) surface is compressed by 8% relative to (111) planes in the bulk, together with earlier results for the Au(001) (Ref. 22) and Au(111) (Ref. 28) surfaces, seems in agreement with this idea. These observations further suggest that the phases of the (001) and (111) surfaces of Au and Pt may be determined by the thermal behavior of an incommensurate, hexagonal-close-packed, metallic monolayer brought into contact with a substrate of square or hexagonal symmetry.[32]

The period of the modulation is given by $2\pi/\delta$, where $\delta$ is the magnitude of the difference wave vector $\boldsymbol{\delta}$. In the aligned phase the modulation lies along the [110] direction, and $\delta$ is simply the product of the incommensurability and $G_1=\sqrt{2}(2\pi/c)$. At 1810 K, $2\pi/\delta=4.9456c/\sqrt{2}=13.96\pm0.02$ Å. Our previous study of the hexagonally reconstructed Au(001) surface revealed that the modulation is a corrugation which penetrates several layers into the substrate.[22] The data presented in this section are consistent with a similar description for the Pt(001) surface. Further evidence which suggests that the structures of the reconstructed Pt(001) and Au(001) surfaces are alike in this regard is provided by the scanning tunneling microscopy (STM) study of Behm *et al.*,[21] which shows a surface corrugation amplitude of $\sim$0.4 Å for the Pt(001) surface. In addition, recent measurements of the specular x-ray reflectivity of the Pt(001) surface[24] indicate a corrugation which is quantitatively comparable to that of the Au(001) surface.[22]

Figure 5 displays the radial width of the peaks shown in Figs. 3 and 4 and of various other peaks characterized at 1810 K. The radial width is smallest ($\sim$0.0009 Å$^{-1}$ FWHM) for wave-vector transfers of about 2 Å$^{-1}$. It increases with increasing wave-vectors transfer, so that the (2,0) hexagonal peak, with a wave-vector transfer of $\sim$5 Å$^{-1}$, shows a radial width of $\sim$0.0045 Å$^{-1}$ FWHM. In addition, the width of the satellite at $\boldsymbol{\delta}$, with a wave-vector transfer of $\sim$0.44 Å$^{-1}$, is 0.0035 Å$^{-1}$ FWHM. The solid line in Fig. 5 shows the radial width expected for our configuration on the basis of an approximate calculation of the resolution function.[37] The solid line provides a good description of the observed radial widths for all of the peaks except for the satellite at $\boldsymbol{\delta}$. In view of the good agreement at larger wave-vector transfers, we believe that the overlayer is translationally well ordered at 1810 K and that the observed radial widths at this temperature represent the radial width of the resolution function. Further work is required to clarify the origin of the discrepancy at small wave-vector transfers. At 1810 K, the observed radial width of the principal hexagonal peak is 0.0014±0.0002 Å$^{-1}$ FWHM, indicating that the

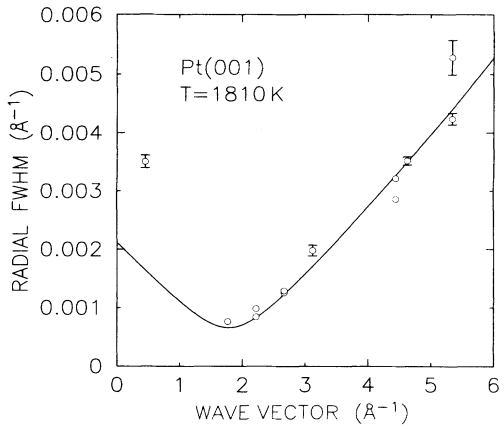


FIG. 5. Width (FWHM) of radial scans taken through various peaks of the Pt(001) surface at 1810 K, plotted vs wave-vector transfer. The solid line corresponds to an approximate calculation of the radial width of the resolution function as described in the text.

extent of translational order in the aligned-hexagonal phase exceeds (5.9/0.00014) Å=4000±600 Å.[38] An improved estimate of the size of the domains of uniform reconstruction follows from consideration of the angular width of the (1,0) hexagonal peak, which is 0.01±0.0002° FWHM, corresponding to a width in reciprocal space of (2.26×0.01/57.3) Å$^{-1}$=0.0004 Å$^{-1}$ FWHM. This is consistent with domains of uniform reconstruction of at least (5.9/0.0004) Å=15,000±3000 Å in size. It is possible to resolve longer length scales in an angular scan because the instrumental resolution in reciprocal space is narrower in the direction transverse to the wave-vector transfer (angular direction) than in the direction alone the wave-vector transfer (radial direction).

### B. Rotated-hexagonal phase

Between 1693 and 300 K, the Pt(001) overlayer exhibits a rotated-hexagonal structure. Figure 6 shows angular scans across the hexagonal rods at (a) (2,0), (b) (0,1), (c) $\tau_1=(1,0)$ and (d) $\tau_2=(-1,2)$, obtained at 1520 K by rotating the crystal about the normal to the scattering plane (rocking curve). In this figure, $\theta=0°$ is the position of the corresponding peak in the aligned-hexagonal phase. For Figs. 6(a) and 6(c), $\theta=0°$ corresponds to the cubic [110] direction; for Fig. 6(d) $\theta=0°$ corresponds to the cubic [110] direction. Evidently, each profile consists of two peaks, symmetrically split about $\theta=0°$. The fact that the angular separation is the same for all of the hexagonal peaks indicates that there are domains of the reconstructed layer which are rotated with respect to the substrate high-symmetry directions. In contrast, the truncation rods (not shown) remain unsplit at all temperatures, confirming that the rotation of the hexagonally reconstructed surface domains is not due to a rotation of the substrate. With reference to Fig. 6, the rotation angle is just the angle at which the hexagonal peaks appear relative to $\theta=0°$—at this temperature, some domains are rotated by 0.8° and the others by −0.8°. The fine structure that can be seen in these scans arises primarily from the

mosaic distribution of crystallites that comprise the sample. A similar fine structure is also evident for the truncation rods.

Figure 7 shows angular scans, also acquired at 1520 K, through the principal hexagonal peak [Fig. 7(b)] and through the satellites, occurring along the [110] direction at $\tau_1+\delta$ [(Fig. 7(a)] and at $\mathbf{G}_1-\delta$ [Fig. 7(c)]. As can be seen from the figure, the angular separation of the satellites is different from that of the principal hexagonal peaks and each is different from the other. This follows from the vector character of the difference wave vector in the rotated-hexagonal phase. Suppose, as illustrated in Fig. 2, that the direction of the (1,0) hexagonal reciprocal lattice vector is rotated by an angle $\theta$ with respect to the direction of the (1,1,0) cubic wave vector. As a result, the difference wave vector is also rotated with respect to the cubic [110] direction. Elementary geometry establishes the relationship between the rotation angle ($\psi$) of the modulation wave vector and the rotation angle of the hexagonal layer:

$$\tan\psi=\tau_1\sin\theta/(\tau_1\cos\theta-G_1)\ , \tag{1}$$

where $G_1$ and $\tau_1$ are the magnitudes of the (1,1,0) cubic wave vector and the (1,0) hexagonal reciprocal lattice vector, respectively.[39] For $\theta=0.8°$ and an incommensurability of 0.2034, $\psi=4.72°$. Therefore, the wave vector which characterizes the modulation (corrugation) is colinear neither with the cubic (1,1,0) wave vector nor with the (1,0) hexagonal wave vector. One may anticipate that the locations of satellites in the rotated phase are given by forming the vector sum of a difference wave vector and either a hexagonal wave vector or a substrate wave vector, corresponding to periodic modulations of the surface layer or substrate, respectively. This is the origin of the different angular separations in Fig. 7. On this basis, it is possible to calculate the angular displacement of the satellites at $\mathbf{G}_1-\boldsymbol{\delta}$ and at $\tau_1+\boldsymbol{\delta}$, which we denote $\psi_1$ and $\psi_2$, respectively. The results are that

$$\tan\psi_1=\tau_1\sin\theta/(2G_1-\tau_1\cos\theta)\ , \tag{2}$$

and

$$\tan\psi_2=2\tau_1\sin\theta/(2\tau_1\cos\theta-G_1)\ . \tag{3}$$

For $\theta=0.8°$ and an incommensurability of 0.2304, we expect $\psi_1=1.21°$ and $\psi_2=1.37°$. These expectations are confirmed by the profiles shown in Figs. 7(a) and 7(c), where the angles in question are indicated by arrows.

There are, of course, two senses of overlayer rotation.

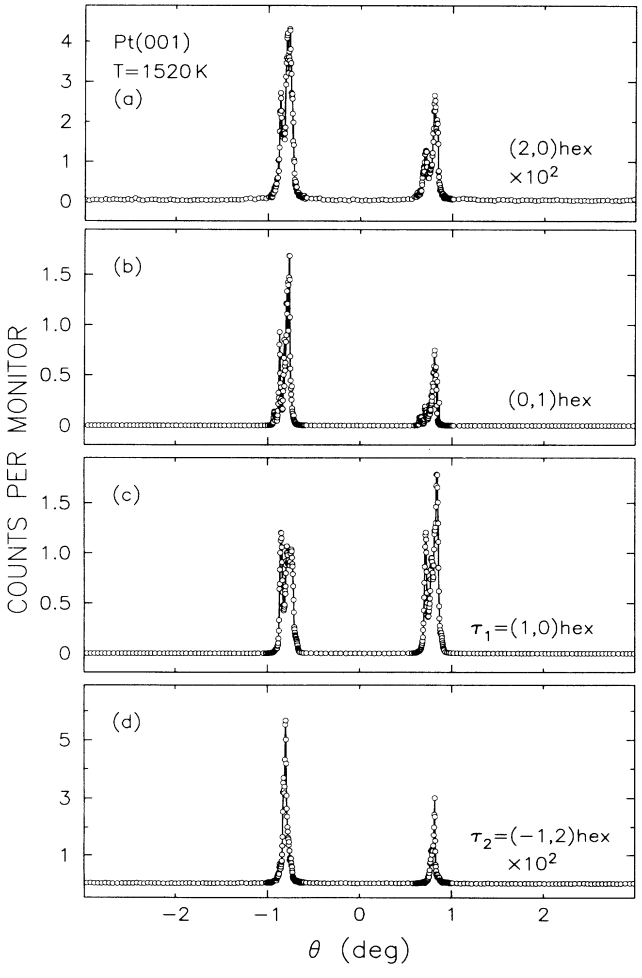


FIG. 6. Angular scans through (a) the (2,0) hexagonal rods, (b) the (0,1) hexagonal rods, (c) the (1,0) hexagonal rods at $\tau_1^+$ and $\tau_1^-$, and (d) the (−1,2) hexagonal rods at $\tau_2^+$ and $\tau_2^-$, in the rotated-hexagonal phase of the Pt(001) surface at 1520 K. The locations of the corresponding rods in the aligned hexagonal phase fall at $\theta=0°$.

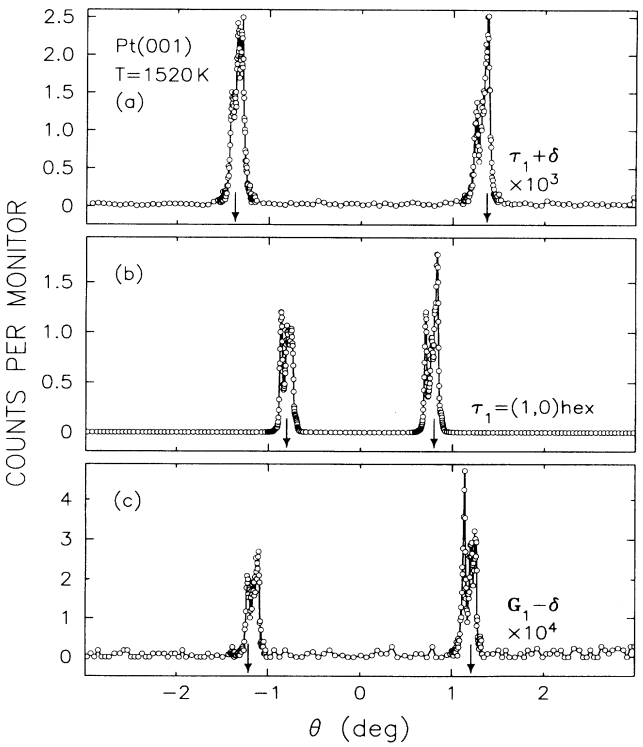


FIG. 7. Angular scans through the (1,0) hexagonal rods at $\tau_1^+$ and $\tau_1^-$ and the satellites at $\tau_1^+ + \boldsymbol{\delta}^+$ and $\tau_1^- + \boldsymbol{\delta}^-$, and at $\mathbf{G}_1-\boldsymbol{\delta}^+$ and $\mathbf{G}_1-\boldsymbol{\delta}^-$. $\theta=0°$ corresponds to the cubic [110] direction. The arrows indicate expected positions of the rods for a rotation angle of the hexagonal overlayer of $\theta=0.8°$.

We denote an arbitrary hexagonal-reciprocal-lattice vector, corresponding to a positive or negative sense of rotation, as $\tau^+$ or $\tau^-$, respectively. Correspondingly, there are two difference wave vectors, which we denote $\delta^+$ and $\delta^-$, respectively. Hexagonal satellites are observed only at $\tau^+ \pm \delta^+$ and at $\tau^- \pm \delta^-$. We have observed no satellites with mixed and positive and negative indices, which is consistent with the idea that a given domain has a definite sense of rotation. Finally, it is important to note that we have verified that away from the [110] direction the locations of satellites are given by the *vector* sum of the difference wave vector ($\delta^{\pm}$), and a hexagonal wave vector ($\tau^{\pm}$) or a lateral substrate wavevector (**G**), as shown in Fig. 2.

### C. Temperature dependence and rotational phase transformation

We turn now to a description of the temperature dependence of the rotation angle of the Pt(001) surface. Results of representative angular scans through the (1,0) hexagonal peak at several temperatures between 1820 and 300 K are shown in Fig. 8. These data were obtained on cooling during a single temperature cycle; however, the results have been reproduced in three separate experiments. At each temperature, the sample was allowed to equilibrate for at least thirty minutes before measurements were made. The sample mosaic for these scans is reflected in the profile of Fig. 8(a), and is also present in scans of the truncation rods (not shown). The mosaic is characterized by one particularly intense peak with a width of 0.01° FWHM, together with a number of much weaker peaks. For temperatures greater than $T_c = 1685$ K, the intense peak is aligned with the cubic [110] direction ($\theta = 0°$). However, on cooling through $T_c = 1685$ K, the peak first appears to broaden and then, with further cooling, to separate into two peaks symmetrically located about the [110] direction. As discussed in Sec. III B, we may identify the angular separation from the [110] direction with a rotation of domains of the overlayer. Between $T_c$ and ~1600 K, the rotation angle increases continuously from 0° to $\theta = \pm 0.7°$. The limit on the maximum possible discontinuity in the rotation angle is 0.05°. For temperatures immediately below $T_c$, the rotated peaks are broader than the sample mosaic (0.01°). However, by ~1640 K the angular widths of the rotated peaks [Fig. 8(d)] reproduce that of the aligned phase. This evolution is evident in Fig. 8: The peaks of Fig. 8(b) are broader than those of Fig. 8(c), which are themselves broader than those of Fig. 8(d). With further decrease of the sample temperature, the rotation angle continues to increase. However, on cooling to ~1580 K (at which temperature $\theta = 0.75°$), additional peaks appear with a slightly larger rotation angle ($\theta = \pm 0.8°$) [Fig. 8(e)], indicating the coexistence of domains of the hexagonal reconstruction with two different rotation angles. In the following, we call the domains that do not rotate "unrotated." Domains with a rotation angle that varies continuously with temperature, we call "continuously rotated;" domains that appear with a rotation angle of 0.8°, we call "discontinuously rotated." As the temperature is decreased from 1580 K, the discontinuously rotated domains retain that orientation. In contrast, the orientation angle of the continuously rotated domains continues to increase smoothly with decreasing temperature. At ~1520 K, there is a single rotation angle of 0.8° [Fig. 8(f)]. However, on further cooling, the orientation of discontinuously rotated domains evolves to slightly smaller angles, so that by 1400 K, their rotation angle is 0.75°.

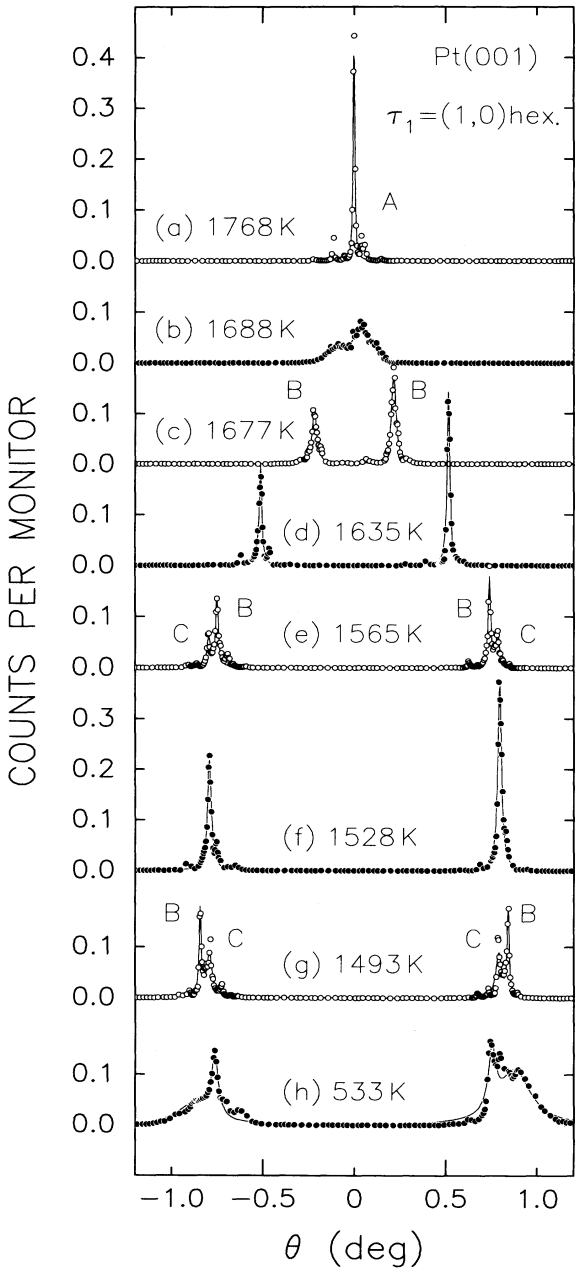


FIG. 8. Angular scans through (1,0) rods of the Pt(001) surface for several temperatures between 1820 and 300 K. Scattering from unrotated domains is indicated by *A*, scattering from continuously rotated domains by *B*, and scattering from discontinuously rotated domains by *C*. Solid lines are fits to a simple model as discussed in the text. The cubic [110] direction corresponds to $\theta = 0°$.

The orientation of continuously rotated domains evolves to larger angles, so that by 1400 K, it is 0.9°. For temperatures below ~1400 K, the peaks at $\theta = \pm 0.9°$ (continuously rotated domains) exhibit a significant angular broadening, but even the peaks at $\theta = \pm 0.75°$ (discontinuously rotated domains) have an angular width larger than in the aligned-hexagonal phase [Fig. 8(h)]. Throughout the temperature range between 1570 and 300 K, there is coexistence among continuously rotated and discontinuously rotated domains.

To extract reliable angular positions and widths, we have fitted the angular scans of Fig. 8, and those obtained at many intervening temperatures, to a model composed of one, two, or four Lorentzians, depending on the temperature. In the aligned-hexagonal phase, a single Lorentzian was used. Its angular width and intensity were independent-fitting parameters. In the rotated-hexagonal phase, either one or two pairs of Lorentzians were used. Each pair was symmetrically located about the [110] direction and we required that the peaks of a given pair have the same angular width. The resultant best-fit profiles are shown as the solid lines in Fig. 8. While such a simple model cannot account for the details of the mosaic structure, it does provide an excellent description of the most intense peaks, except at the lowest temperatures, where the distribution of angles is more complicated than can be well described by four Lorentzians [Fig. 8(h)]. Nevertheless, even at these temperatures, the model captures the main features of the angular profiles.

Figure 9 shows three radial scans through the (1,0) hexagonal peak, which are typical of those obtained at temperatures between 1810 and 300 K. The scan taken at 1766 K was obtained in the aligned-hexagonal phase, while the scans taken at 1631 and 520 K were obtained in the rotated-hexagonal phase. With decreasing temperature, the peak is displaced to larger wave vectors. Thus, it is clear that the incommensurability along the [110] direction increases with decreasing temperature. Radial scans through the $(-1,2)$ hexagonal peak (not shown) establish that, in contrast, the incommensurability decreases along the $[1\bar{1}0]$ direction with decreasing temperature. It is further apparent from Fig. 9 that the radial width of the principal hexagonal peak at 520 K is approximately twice what it is at 1631 or 1766 K. The radial width of the $(-1,2)$ hexagonal peak is also increased at lower temperatures. It follows that the extent of translational order decreases with decreasing temperature. Similar behavior was observed for the hexagonally reconstructed Au(001) surface.[22]

Figure 10(a) shows the temperature dependence of the rotation angles of the unrotated (squares), continuously rotated (open circles), and discontinuously rotated (closed circles) domains. For temperatures between 1820 K and $T_c = 1685$ K, the overlayer is aligned with high-symmetry directions of the substrate. Between 1685 and ~1590 K, the overlayer has a single rotation angle which varies smoothly with temperature from 0° to 0.75°. At ~1590

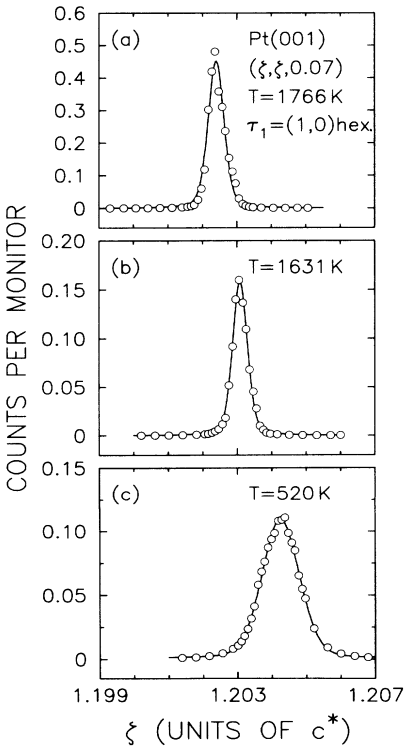


FIG. 9. Typical radial scans through (1,0) hexagonal rod of the Pt(001) surface at three temperatures.

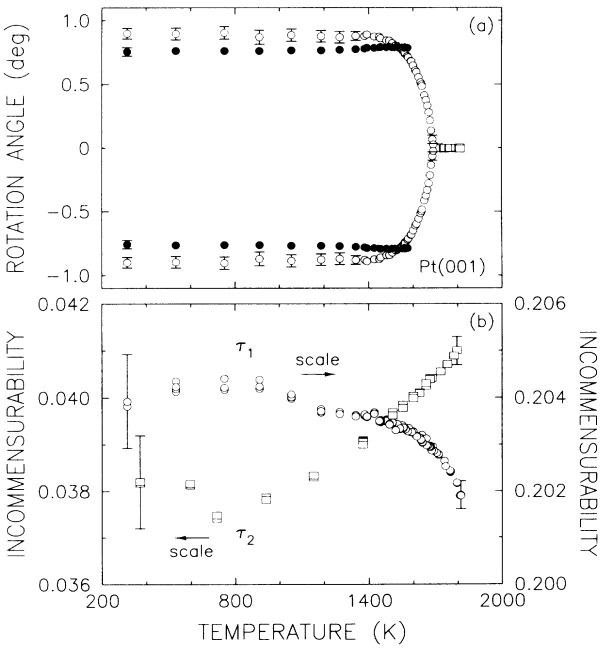


FIG. 10. Temperature dependence of the rotation angles and incommensurabilities of the Pt(001) overlayer. (a) Open squares correspond to unrotated domains, open circles correspond to continuously rotated domains, and closed circles correspond to discontinuously rotated domains. The rotation angles were determined by the fits shown in Fig. 8 and are described in the text. Error bars denote the angular FWHM of the corresponding peak. (b) Incommensurabilities of the hexagonal overlayer in the cubic [110] direction (open circles) $\tau_1/G_1 - 1$ and the cubic $[1\bar{1}0]$ direction (open squares) $\tau_2/G_2 - 1$.

K, additional scattering is evident at a rotation angle of 0.8°, corresponding to the appearance of discontinuously rotated domains in coexistence with the population of continuously rotated domains. Between ~1590 and 1400 K, the rotation angle of continuously rotated domains continues to increase, finally reaching a value of 0.9°. The rotation angle of discontinuously rotated domains decreases slightly between ~1590 and 1400 K, at which temperature it is ~0.75°. Between ~1400 and 300 K, both rotation angles are approximately constant.

Figure 10(b) summarizes the corresponding temperature dependence of the incommensurabilities along the [110] direction (open circles) and along the $[1\bar{1}0]$ direction (open squares). The incommensurability along the $[1\bar{1}0]$ direction is 0.0410 ±0.0003 at 1820 K and decreases smoothly with decreasing temperature reaching a value of 0.038±0.001 at 300 K. In the same temperature range, the incommensurability along the [110] direction increases smoothly from 0.2022±0.0003 at 1820 K to 0.204±0.001 at 300 K. There is no obvious high-order commensurate structure within this range of values of the incommensurability. The fact that the incommensurability varies continuously as a function of temperature is further evidence that the hexagonal layer is truly incommensurate. A high-order commensurate structure would likely give rise to an incommensurability which is observably locked to a fixed value. For temperatures between 1685 and 1580 K, for which there is a single rotation angle that varies from 0° to 0.75° (continuously rotated domains), the incommensurability along [110] direction varies from ~0.2028 to ~0.2032—a relative change of only ~0.2%. The evolution of the incommensurabilities illustrated in Fig. 10(b) corresponds to a slight distortion of the hexagonal unit cell. It is worth noting, however, that the areal density of the hexagonal layer relative to the areal density of planes in the crystal interior is nearly constant between 1820 and 300 K. At 300 K, the average unit cell dimensions are as follows: $a$ =2.664±0.003 Å, $b$ =2.673±0.003 Å, $\gamma$ =120.11°±0.05°, and the period of

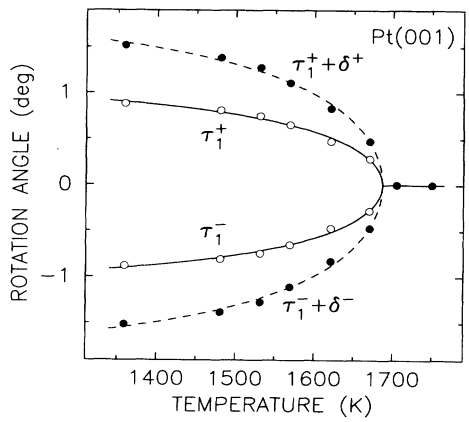


FIG. 11. Temperature dependence of the rotation angles of the (1,0) hexagonal rods at $\tau_1^+$ and $\tau_1^-$ (open circles) and of the satellites at $\tau_1^+ + \delta^+$ and $\tau_1^- + \delta^-$ (filled circles). The solid line is a parametrization of the temperature dependence of the hexagonal rods. The dashed line is calculated from that parametrization with the use of Eq. (3).

the surface corrugation along the difference wave vector $\delta$ is $4.90c/\sqrt{2}$=13.60 Å.

It is also of interest to ascertain the variation of the corrugation rotation angle with temperature. In Fig. 11, the rotation angle of the (1,0) hexagonal peak ($\tau_1^{\pm}$) (open circles) is shown together with the angular location of the satellite peaks at $\tau_1^+ + \delta^+$ and $\tau_1^- + \delta^-$ (filled circles) for temperatures between 1750 and 1350 K. The solid line in Fig. 11 is a parametrization of the rotation angle of the principal hexagonal peak. The corresponding angular displacement of the satellite peak is calculated using Eq. 3 and shown by the dashed line in Fig. 11. Evidently, there is good agreement between the measured angular position of the satellites and the dashed line. We may infer, therefore, that the corrugation wave vector also rotates smoothly with temperature in the manner expected (Eq. 1). At 300 K, the corrugation rotation angle is $\psi$=5.3° for continuously rotated domains ($\theta$=0.9°) and $\psi$=4.4° for discontinuously rotated domains ($\theta$=0.75°).

Our measurements of the average unit cell dimensions, the relative rotation angle of the hexagonal layer, the period of the surface corrugation and its rotation angle may be compared to the results of previous studies. The low-energy electron diffraction study of Heinz, Heilmann, and Müller[19] was performed at temperatures between 1400 and 77 K. Throughout this temperature range, the annealed, clean Pt(001) surface was found to have a hexagonal structure, to the accuracy of the experiment, with a lattice constant contracted by 4% with respect to the bulk nearest-neighbor distance. In addition, it was determined that the relative rotation angle of the hexagonal layer was $\theta$=0.7°±0.2°. In the STM study of Behm *et al.*,[21] which was carried out at 500 K, the clean, hexagonally reconstructed Pt(001) surface was found to exhibit a surface corrugation with a period of 14 Å. The corrugation was further found to be oriented at about $\psi$=±5° to the substrate [110] direction. Our x-ray results are in excellent agreement with the results of both of these studies. The x-ray measurements, however, are more precise.

Figure 12(a) shows the magnitude of the rotation angle of the continuously rotated domains, plotted on a logarithmic scale versus reduced temperature (also plotted on a logarithmic scale). It is evident from the linear behavior in Fig. 12(a) that the rotation angle varies with a power-law dependence on reduced temperature between 0.002 and 0.06. For smaller reduced temperatures the peak broadening prevents quantitative analysis. At larger reduced temperatures there are two rotation angles. For reduced temperatures in the range between 0.002 and 0.06, we have fitted the rotation angle to a power law: $\theta = A[(T_c - T)/T_c]^{\beta}$. The parameters varied in the fit were $\beta$, $T_c$, and $A$. An accurate description of the data in this temperature range is provided by the values $\beta$=0.47±0.05, $T_c$=1685±10 K, and $A$ =2.65°±0.4°, as shown by the solid line in Fig. 12(a). Figure 12(b) illustrates the power-law fit on linear axes, and includes the observed rotation angles of the unrotated continuously rotated, and discontinuously rotated populations. Deviations from the power law occur when the surface shows two distinct rotation angles. The ob-

served variation of the rotation angle with reduced temperature—specifically, the fact that the exponent $\beta$ equals one-half to within the error—is consistent with a mean-field description of the rotational transformation.

We next summarize our results for the temperature dependence of the radial widths of the (1,0) and the $(-1,2)$ hexagonal rods, at $\tau_1$ and $\tau_2$, respectively, and of the substrate (1,1,0) and $(2,-2,0)$ truncation rods, at $\mathbf{G}_1$ and $\mathbf{G}_2$, respectively. These data, collected during two separate cooling cycles, are shown in Fig. 13(a). On one of the temperature cycles, the radial widths of the hexagonal (1,0) and the cubic (1,1,0) rods were measured. On the other cycle, the widths of the hexagonal $(-1,2)$ and the cubic $(2,-2,0)$ rods were measured. In each case, for temperatures between 1820 and $\sim$1400 K, the radial width is indistinguishable from that expected on the basis of the diffractometer resolution (Fig. 5). For temperatures decreasing from 1400 to 300 K, however, the radial peak width of the hexagonal peak at $\tau_1$ increases smoothly. At 300 K, its radial width is $0.0028\pm0.0002$ Å$^{-1}$ FWHM, which is significantly larger than its width at 1400 K of $0.0014\pm0.0002$ Å$^{-1}$ FWHM. Assuming that the reconstructed surface is composed of domains each of a finite size, then the deconvolved radial width of the (1,0) hexagonal rod at $\tau_1$ is $\sqrt{(0.0028)^2-(0.0014)^2}$ Å$^{-1}=0.0024\pm0.0004$ Å$^{-1}$ FWHM. Such a value corresponds to an average domain size of $2400\pm400$ Å.[38] In the case of the $(-1,2)$ hexagonal rod at $\tau_2$, the radial width also increases smoothly for temperatures decreasing from 1400 to 700 K. At 700 K, its radial width is $0.005\pm0.0005$ Å$^{-1}$ FWHM, so that the deconvolved width is $\sqrt{(0.005)^2-(0.004)^2}$ Å$^{-1}=0.003\pm0.001$ Å$^{-1}$ FWHM at 700 K, which corresponds to an average domain size of $2000\pm700$ Å.[38] Below 700 K, the radial width of the $(-1,2)$ hexagonal rod is significantly increased to $0.007\pm0.001$ Å$^{-1}$ FWHM, giving a domain size of only $1000\pm200$ Å. The discrepancy between the domain size at 300 K determined on the basis of the radial width of the $(-1,2)$ rod and that determined on the basis of the radial width of the (1,0) rod, suggests that the domain size may depend sensitively on the thermal history of the sample. Such issues are discussed further in the Appendix. The radial widths of the substrate rods show no significant change between $\sim$1400 and 300 K, and we observe no difference between the radial widths for the continuously rotated and discontinuously rotated populations at any temperature. In the STM study of Behm *et al.*,[21] which was performed at 500 K, it was found that regions of uniform hexagonal reconstruction with linear dimensions of several hundred to several thousand Angstroms were separated by monoatomic or biatomic steps. It is thus possible that the increase of the radial width of the hexagonal rods coincides with the formation of an increasing density of surface steps.[40]

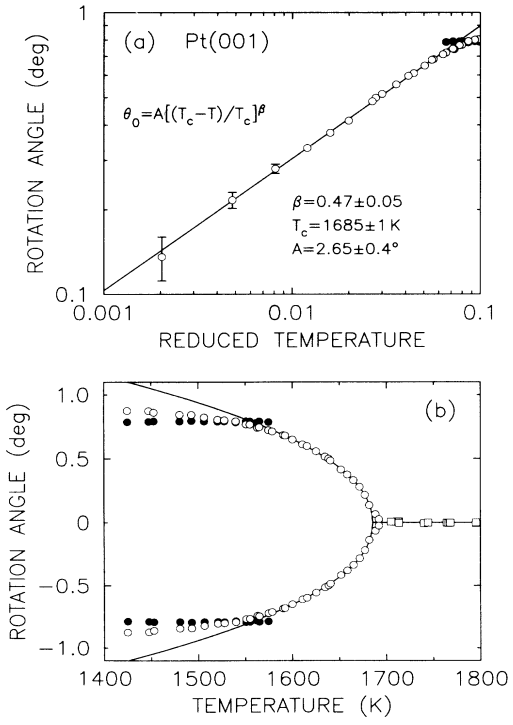


FIG. 12. Rotation angle as a function of temperature for the Pt(001) surface. (a) Log-log plot of rotation angle vs reduced temperature $[(T_c-T)/T_c]$. The solid line is a fit to a power law for $0.002<(T_c-T)/T_c<0.06$. (b) Linear plot showing rotation angles for all of the rotated domains. The solid line corresponds to the power-law fit.

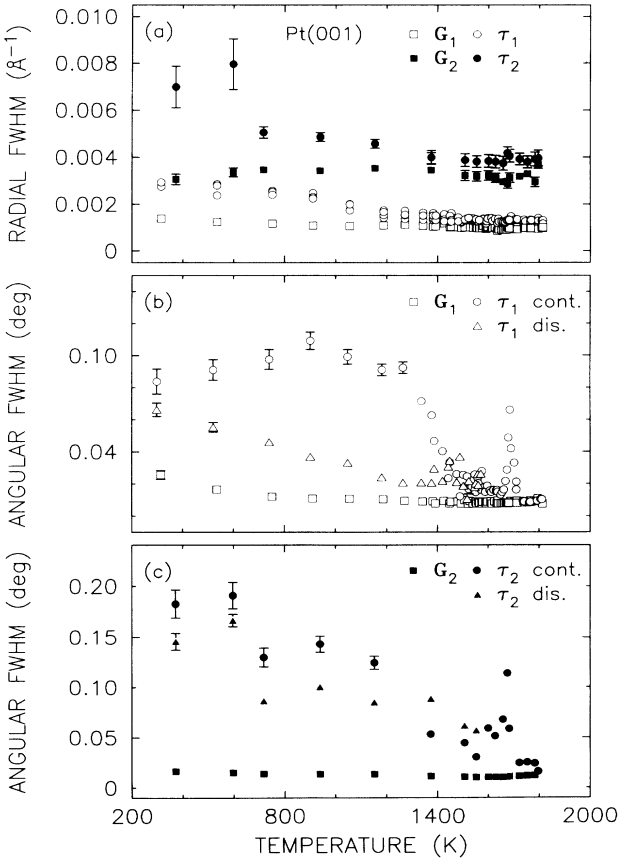


FIG. 13. Temperature dependence of the radial [(a)] and angular [(b) and (c)] widths for hexagonal and substrate rods along the cubic [110] and [1$\bar{1}$0] directions.

A decreasing translational order with decreasing temperature is a striking and unexpected aspect of both the Pt(001) and Au(001) surfaces.[22] Recently, Alerhand *et al.*[33] have proposed that reconstructed, high-symmetry surfaces, which can reconstruct into one of a number of rotationally equivalent structures and which have an anisotropic stress tensor, are unstable to the formation of finite-sized domains. The origin of domain formation is the accompanying reduction of elastic stress. Surfaces for which this behavior is possible include the $(2\times1)$ reconstructed Si(001) surface[33,41] and the Au(111) surface.[28,42–44] Just as for the $(2\times1)$ reconstructed Si(001) surface, it may be that for the Pt(001) and Au(001) surfaces, the elastic energy is smaller for smaller domains of the hexagonal reconstruction. In this regard, we note that the corrugation of the Pt(001) and Au(001) surfaces may lead to a large anisotropy in the surface stress tensor. The energetic gain from the formation of small domains competes against the cost of creating surface steps. The competition between these two contributions determines the domain size. The reason the domain size should decrease with decreasing temperature remains unexplained.

We now present the results of measurements of the angular widths of the various peaks. Figure 13(b) shows the angular widths of the (1,0) hexagonal rod at $\tau_1$ (open circles and open triangles for the continuously and discontinuously rotated domains, respectively), and of the (1,1,0) substrate rod at $\mathbf{G}_1$ (open squares). Figure 13(c) shows the angular widths of the $(-1,2)$ hexagonal rod at $\tau_2$ (solid circles and solid triangles for the continuously and discontinuously rotated populations, respectively), and of the $(2,-2,0)$ substrate rod at $\mathbf{G}_2$ (solid squares). The angular width of the substrate rods is determined by the sample mosaic, which increases with decreasing temperature from 0.01° FWHM at 1820 K to 0.02° FWHM at 300 K. The angular widths of the hexagonal rods show a much stronger temperature dependence. Above $T_c$, the angular width of the (1,0) hexagonal rod at $\tau_1$ is equal to the sample mosaic. At and immediately below $T_c$, there is an increase. On further cooling, the angular width decreases again and nearly reproduces its value above $T_c$. We attribute the variation of the width near the nominal $T_c$ to the existence of a distribution of slightly different transformation temperatures for different domains across the surface. At $\sim$1350 K, the angular width of the continuously rotated (1,0) hexagonal rod increases precipitously to reach 0.1° FWHM at 1250 K, a value which it maintains between 1250 and 300 K. In contrast, the angular width of the discontinuously rotated (1,0) hexagonal rod increases gradually from $0.01\pm0.002$° FWHM at 1590 K to $0.07\pm0.01$° FWHM at 300 K. An angular width of $0.07\pm0.01$° FWHM corresponds to a width in reciprocal space of $0.0028\pm0.0004$ Å$^{-1}$ FWHM. This is consistent with domains of uniform reconstruction of $2000\pm300$ Å in size. Thus the increase in the angular width of discontinuously rotated rods is consistent with the decrease in translational order, deduced above from the behavior of the radial width of the (1,0) hexagonal rod. The angular width of the continuously rotated (1,0) hexagonal rod cannot be understood in the same way. Instead, we infer a distribution of rotation angles for the continuously rotated domains. With regard to the $(-1,2)$ hexagonal rods at $\tau_2$ [Fig. 13(c)], the angular width below $T_c$ does not reproduce its value above $T_c$. Rather, it stays at $\sim$0.06° FWHM between $T_c$ and 1300 K, and then increases to $\sim$0.1° FWHM for discontinuously rotated rods and $\sim$0.15° FWHM for continuously rotated rods. For the temperature cycle during which the $(-1,2)$ rods were studied, typical temperature steps of 30 K were taken through the transformation; for the temperature cycle during which the (1,0) rods were studied, typical temperature steps of 5 K were taken. We believe that the difference between the angular widths observed on the two different cycles probably results from the different cooling rates employed in each case. (See Appendix).

## IV. GOLD (001) SURFACE—RESULTS AND DISCUSSION

In earlier studies of the Au(001) surface,[22] we observed disordered, aligned-hexagonal, and rotated-hexagonal phases, which are similar in many respects to the corresponding phases of the Pt(001) surface. However, the rotational transformation of the hexagonally reconstructed Au(001) surface was found to be discontinuous, contrary to the behavior observed in the Pt(001) surface. In addition, unrotated domains were always observed in coexistence with rotated domains. Furthermore, the so-called unrotated domains appeared to exhibit a distribution of rotation angles (about zero), the width of which was found to increase with decreasing temperature. For these reasons, and in view of our study of the orientational behavior of the Pt(001) surface (Sec. III), we decided to reexamine the orientational epitaxy of the hexagonally reconstructed Au(001) surface. The results of this investigation are described in the present section.

Figure 14 shows the results of typical angular scans through the (1,0) hexagonal peak of the reconstructed Au(001) surface for temperatures from 1100 to 300 K. In the figure, $\theta=0$° corresponds to the cubic [110] direction. As in Ref. 22 and Sec. III, measurements were performed either by monotonically lowering the temperature from the disordered phase or by monotonically raising the temperature from 300 K. At each temperature, the sample was allowed to equilibrate for $\sim$30 min before measurements were performed. The principal difference between the experiments reported here and those of Ref. 22 is that finer temperature steps (30 K) were taken in the present experiment. (See Appendix).

For temperatures greater than $\sim$1000 K, the angular profile consists of a single peak which is aligned with the cubic [110] direction. However, on cooling to 993 K [Fig. 14(b)], there is a noticeable increase in the width of the peak at $\theta=0$°. Furthermore, at this temperature, it is possible to discern two additional peaks, which are displaced symmetrically about the cubic [110] direction by $\pm0.84$°. At 963 K [Fig. 14(c)], the rotated peaks at $\pm0.84$° are unchanged in position, but are more intense than at 993 K. Meanwhile, the unrotated peaks have acquired pronounced "shoulders." At 930 K [Fig. 14(d)],

the peaks at $\pm 0.84°$ have intensified, but the most striking evolution has occurred for the unrotated peak and its shoulders, which are now more pronounced and clearly suggestive of two further peaks of unequal intensity displaced by about $\pm 0.3°$ from the [110] direction. By 904 K [Fig. 14(e)], the peaks at $\theta = \pm 0.84°$ are still more intense than at 930 K. However, the peaks, which occurred at $\sim 0.3°$ for 930 K, have moved to $\theta = \pm 0.4°$ and are weaker in intensity than at 930 K. Between 904 and 870 K [Fig. 14(f)] the intensities of the peaks at $\theta = \pm 0.4°$ are further diminished, while those of peaks at $\theta = \pm 0.84°$ continue to increase. On further cooling, the intensity of the unrotated peak becomes noticeably weaker and, by 759 K [Fig. 14(g)], new shoulders are evident on the large-angle sides of the peaks at $\theta = \pm 0.84°$. These trends continue with further cooling so that by 435 K, the intensity of the unrotated peak is yet weaker and the new shoulders are more pronounced. At any given temperature, the angular profile at the (0,1) hexagonal position qualitatively reproduces that at the (1,0) position. This is shown in Fig. 15 for a temperature of 904 K. The most straightforward interpretation of these data is that there is coexistence among domains of the hexagonal reconstruction with several different rotation angles.

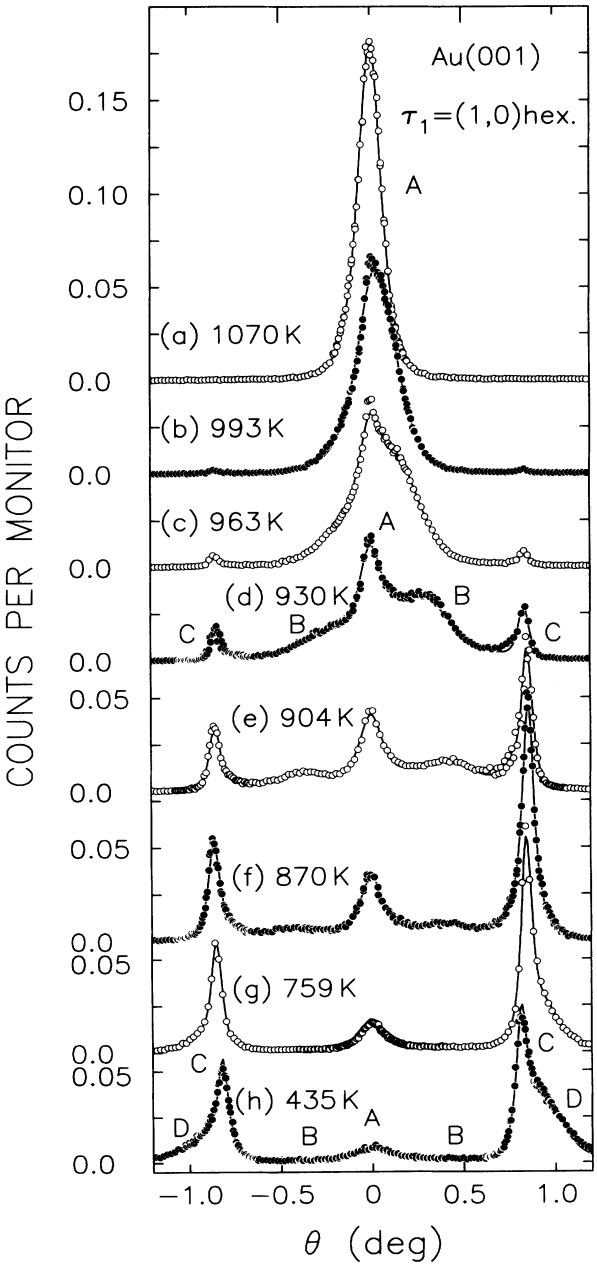


FIG. 14. Angular scans through the (1,0) hexagonal rods of the Au(001) surface for several temperatures. Scattering from unrotated domains is labeled *A*, from continuously rotated domains *B*, from 0.84°-rotated domains *C*, and from 0.9°-rotated domains *D*. Solid lines are fits to a simple model as described in the text. The cubic [110] direction corresponds to $\theta = 0°$.

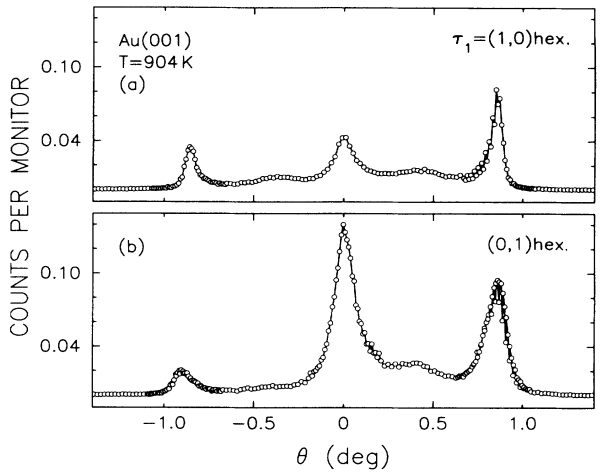


FIG. 15. Angular scans at (a) the (1,0) and (b) (0,1) hexagonal positions at 904 K.

To characterize the profiles of Fig. 14, we have fitted the data to a model which consists of up to seven Lorentzians. To minimize, as far as possible, the number of fitting parameters, we again restricted consideration to one unrotated peak, together with three pairs of rotated peaks. Each pair of peaks was symmetrically located about the cubic [110] direction and we required that peaks of a given pair have the same angular width. In addition, the widths of the peaks at $\pm 0.84°$ were fixed at 0.04° FWHM and the width of the unrotated peak was fixed at 0.09° FWHM. The fitting parameters, therefore, were the amplitudes of seven peaks, the angular displacements of the three pairs, and the widths of two of the pairs. The solid lines in Fig. 14 show the best-fit model curves, which are in excellent agreement with the experimental profiles.

The various rotation angles determined by the fits, together with the incommensurabilities of the Au(001) surface along the [110] and [1$\bar{1}$0] directions of the substrate[22] are shown in Fig. 16. An unrotated component is present at all temperatures (open squares). In addition, there are three distinct, rotated components which can coexist. One is composed of continuously rotated domains (open circles), the rotation angle for which varies from 0° to 0.5°. Regarding the other two components, one shows a rotation angle that is roughly constant at 0.84° ("0.84°-rotated" domains, shown as filled circles) and the other a rotation angle that seems to vary

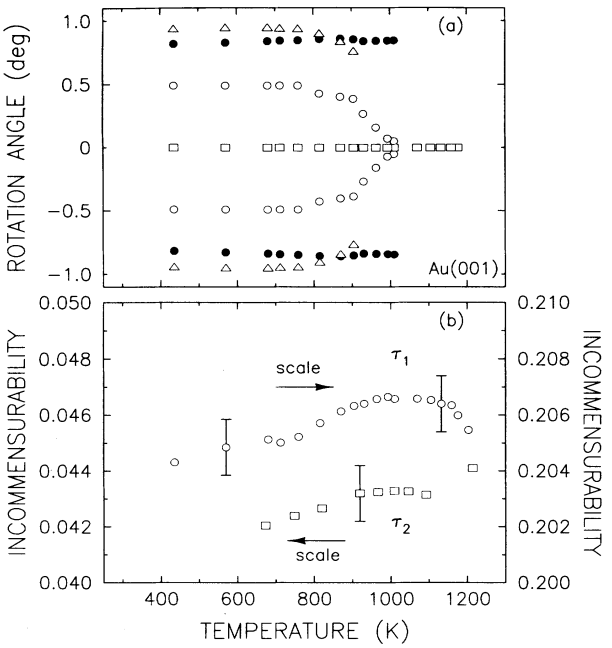


FIG. 16. Temperature dependence of the rotation angles and incommensurabilities of the Au(001) overlayer. (a) Squares (unrotated domains), open circles (continuously rotated domains), filled circles (0.84°-rotated domains) and triangles (0.9°-rotated domains) indicate the rotation angles from the fits shown in Fig. 15. (b) Incommensurabilities of the hexagonal overlayer in the cubic [110] direction (open circles) and [1$\bar{1}$0] direction (open squares).

from ~0.75° to ~0.9° ("0.9°-rotated" domains, shown as open triangles). For temperatures less than ~770 K, the continuously rotated component is very weak in intensity and broad. Nevertheless, eliminating these peaks from the model significantly diminishes the quality of the fits, even for temperatures less than ~770 K. The incommensurabilities of the Au(001) surface [Fig. 16(b)] show little variation with temperature in the [110] and [1$\bar{1}$0]directions. Thus, as is the case for the Pt(001) surface, the areal density of the surface layer changes little from 1200 to 300 K.

Figure 17(a) displays the angular widths of the various peaks shown in Fig. 14 as a function of temperature. In Fig. 17(a), the widths of unrotated peaks are shown as open squares; those of continuously rotated peaks are shown as open circles; those of 0.84°-rotated peaks are shown as filled circles, and those of 0.9°-rotated peaks are shown as open triangles. In Fig. 17(b), the integrated intensities of unrotated peaks are shown as open squares; those of continuously rotated peaks are shown as solid circles; and those of 0.9° rotated peaks are shown as open triangles. The fitted width of the 0.9°-rotated peaks is approximately temperature independent (0.11° FWHM). On the other hand, the width of continuously rotated peaks is ~0.1° FWHM at ~1000 K and becomes much larger with decreasing temperature, reaching ~0.6° FWHM by 400 K. However, the peak intensities of the continuously rotated components are very weak for temperatures below ~770 K.

One of the most remarkable results of the present study is the observed correspondence between the surface phase behavior of the Au(001) surface and that of the Pt(001) surface. Figure 18 shows a comparison between the various rotation angles observed for the Au(001) surface [Fig. 18(a)] and those of the Pt(001) surface [Fig. 18(b)]. In each case, the temperature is expressed as a fraction of the bulk melting temperature, which is 1337 K for Au and 2045 K for Pt. While there are significant

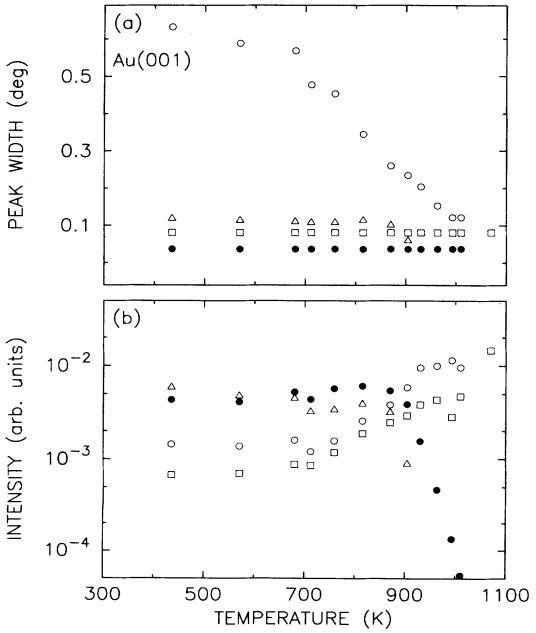


FIG. 17. Temperature dependence of (a) the angular width and (b) peak intensity for different domain types determined by the fits shown in Fig. 15.

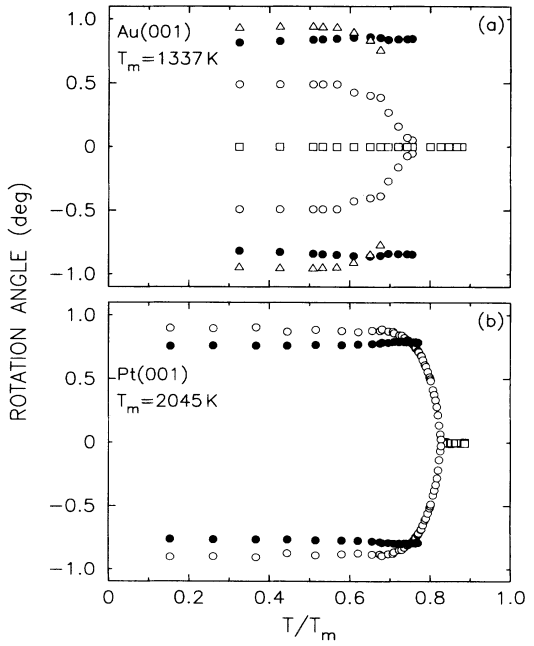


FIG. 18. Comparison of temperature dependence of the rotation angles of the hexagonally reconstructed (a) Au(001) and (b) Pt(001) surfaces. The temperature is expressed as a fraction of the bulk melting temperature (1337 K for Au and 2045 K for Pt).

differences between the two plots, there are also striking similarities. The absence of data points for temperatures greater than $0.9T_m$ for Au(001) and Pt(001) corresponds in both cases to the absence of the hexagonal reconstruction in this temperature range—the surfaces are disordered.[22,24] The disappearance of the reconstruction peak occurs within a temperature step of $\sim 5$ K, the smallest possible with the sample heating arrangement. Both surfaces show an aligned-hexagonal phase (zero rotation angle) at temperatures immediately below the transformation from the disordered phase. In the case of the Pt(001) surface, the rotation angle initially increases smoothly with temperatures decreasing from a critical temperature of $0.85T_m$; eventually, it saturates at $\sim 0.87°$ [open circles in Fig. 18(b)]. At $0.77T_m$, an additional rotation angle (0.8°) appears, which decreases slightly to $\sim 0.77°$ at lower temperatures [filled circles in Fig. 18(b)]. For the hexagonal reconstruction of the Au(001) surface, on cooling, rotated domains appear first at $0.74T_m$ with a rotational angle of 0.84° [filled circles in Fig. 18(a)]. A continuously rotated component also emerges at $0.74T_m$ and its rotation angle increases smoothly with decreasing temperature. Clearly, the transformation temperatures in units of $T_m$ and certain of the observed rotation angles are remarkably similar for the Au(001) and Pt(001) surfaces. The coexistence of domains with different rotation angles is also common to the two surfaces. Both display rotational behavior that may be characterized as continuous and behavior that may be characterized as discontinuous. The principal difference appears to be that the rotational transformation of the Pt(001) surface is mainly continuous, while, for the Au(001) surface, it is strongly discontinuous. With regard to the correspondence between the phase behaviors of the Pt(001) and Au(001) surfaces, we note that the electronic band structures of the Au and Pt are closely similar,[30] in spite of their very different bulk melting temperatures.

## V. MEAN-FIELD THEORY OF ROTATIONAL TRANSFORMATION

Novaco and McTague considered an incommensurate, hexagonal monolayer adsorbed on a rigid, hexagonal substrate at zero temperature. They pointed out that, while the interfacial energy does not depend on the translational registry between the overlayer and the substrate, it does depend on their relative orientation. Specifically, they predicted that the interfacial energy is minimized for a relative orientation which is different from the high-symmetry directions of the overlayer or of the substrate, and which depends approximately linearly on the incommensurability. The proportionality constant is determined by the frequencies of the overlayer lattice vibrations. For an incommensurability of $\sim 0.2$, as observed along the [110] direction for the Pt(001) and Au(001) overlayers, the linear response calculations of Novaco and McTague should apply,[1,25,26] and in the simplest case a rotation angle of about 7° is predicted. [Novaco and McTague considered a hexagonal overlayer on a hexagonal substrate. The (001) surface layers of Pt and Au are hexagonal on square substrates. However, because we *assume* that a single Fourier component dominates the overlayer-substrate interaction, once that Fourier component is chosen, their results carry over to the present case.] A rotation angle of 7° is nearly a factor of 10 larger than any of the observed rotation angles of the Pt(001) overlayer. Moreover, in the temperature range (between 1685 and 1580 K) in which the Pt(001) overlayer exhibits a single rotation angle, varying continuously from 0° to 0.75°, the incommensurability along the [110] direction increases by only 0.0005. With regard to the possibility that the incommensurability along the $[1\bar{1}0]$ direction determines the rotation angle, we note that no satellites associated with this incommensurability are observed. It is further worth noting that the incommensurability along the $[1\bar{1}0]$ direction decreases slightly as the rotation angle increases. On this basis, the possibility that the *change* in the incommensurability along the $[1\bar{1}0]$ direction is responsible for the Pt(001) rotational transformation may be discounted within the context of the theory of Novaco and McTague or related theories.[25,26] [As noted earlier, the area per atom within the hexagonally reconstructed Pt(001) surface layer is approximately constant.]

It is evident that our results are inconsistent with several of the predictions of Novaco and McTague. We believe that the discrepancies originate from three assumptions. First, the theory of Novaco and McTague assumes that pair potentials can be used to describe the interactions among the surface and substrate atoms. Unlike the rare gases adsorbed on graphite, for which pair potentials provide a good description of the interatomic interactions, such an approach fails to account for metallic binding, nor can it explain metal surface reconstructions.[27] Second, Novaco and McTague take the substrate to be rigid and any atomic displacements to be small. In contrast, our results show that the Au(001) surface is strongly coupled to the substrate through the corrugation.[22] [We infer a similar corrugation at the Pt(001) surface.] Third, their calculations are carried out assuming that the temperature is zero.

Recently, Grey and Bohr[45] have argued that a low-energy orientation could occur whenever a modulation wave vector is parallel to any substrate or any overlayer reciprocal-lattice vector.[8,45–47] For the Pt(001) and Au(001), however, the corrugation wave vector is not aligned parallel to a substrate or to an overlayer reciprocal-lattice vector. Thus, we believe it to be unlikely that the observed rotation angles will be understood on this basis.

The fact that the rotation angle of the hexagonally reconstructed Pt(001) surface follows a one-half-power law versus reduced temperature motivates a mean-field description of the phase transformation. In the following, we present a simple mean-field theory of rotational transformations. For the case that there are two symmetrical minima in the orientation dependence of the interfacial energy, it has been suggested[5,9] that a temperature-driven rotational transformation might show the same critical behavior as the two-dimensional Ising model: $\theta = A[(T_c - T)/T_c]^{1/8}$. However, an important aspect of our theory is that the amplitude of an

orientational mode does not diverge as the transformation temperature is approached and as the wave vector of the mode goes to zero. This result indicates that rotational transformations may, in general, be well described by mean-field theory. The basis of this statement is the observation that acoustic phonons provide the appropriate fluctuation modes to consider at a rotational transformation. A similar proposal has been made previously in the context of structural phase transformations at which a homogeneous deformation of the unit cell is the primary order parameter.[48]

We start by writing a Hamiltonian for the long-wavelength translational and orientational degrees of freedom of a hexagonal overlayer:

$$H=\frac{\Omega}{2}\sum_{\mathbf{K}\,(\neq 0)}\{\mu K^2\mathbf{u}(\mathbf{K})\cdot\mathbf{u}(-\mathbf{K})+(\mu+\lambda)[\mathbf{K}\cdot\mathbf{u}(\mathbf{K})]\times[\mathbf{K}\cdot\mathbf{u}(-\mathbf{K})]\}+\int d^2\mathbf{r}(-\tfrac{1}{2}v\theta^2+\tfrac{1}{4}w\theta^4)\ . \tag{4}$$

The first term describes the energy associated with displacements $[\mathbf{u}(\mathbf{r})]$ of the overlayer atoms from their positions on an ideal, hexagonal lattice, and $\mathbf{u}(\mathbf{K})$ is the amplitude of the displacement mode of wave vector $\mathbf{K}$. The quantities $\lambda$ and $\mu$ are Lamé coefficients, and $\Omega$ is the overlayer area. This contribution is identical to that written by Nelson and Halperin (Ref. 49, Eq. 5.12). We have added to this the second term, which gives the interfacial energy as a function of the overlayer orientation $[\theta(\mathbf{r})]$ at a position $\mathbf{r}$ within the overlayer. We have chosen a specific form for the interfacial energy with two equal minima, which are symmetrically placed at $\theta=\pm\sqrt{v/w}$ about $\theta=0°$. The parameters $v$ and $w$ are to be determined from a microscopic theory—this form of the interfacial energy approximates that predicted by Novaco and McTague with suitable expressions for $v$ and $w$. In this sense, our calculation is merely an extension to nonzero temperature of any theory which yields an explicit prediction for $v$ and $w$. It is convenient to rewrite the first contribution in terms of the local orientation of the overlayer, using the relationship between orientation and displacement: $\theta(\mathbf{K})=i\mathbf{K}\times\mathbf{u}(\mathbf{K})/2$. Then

$$\mathcal{H}=\frac{\Omega}{2}\sum_{\mathbf{K}\,(\neq 0)}\{(2\mu+\lambda)[\mathbf{K}\cdot\mathbf{u}(\mathbf{K})][\mathbf{K}\cdot\mathbf{u}(-\mathbf{K})]+4\mu\theta(\mathbf{K})\theta(-\mathbf{K})\}+\int d^2\mathbf{r}(-\tfrac{1}{2}v\theta^2+\tfrac{1}{4}w\theta^4)\ . \tag{5}$$

The first term of the sum in Eq. (5) is the energy of the longitudinal phonons and the second term is the energy of the transverse phonons, written in terms of the corresponding orientational modes. Each of these terms corresponds to different, independent normal modes of the overlayer. Therefore, for a discussion of rotational transformations, we need to consider only the transverse modes—the long wavelength longitudinal modes may be neglected. To allow for a nonzero, mean rotation angle $(\theta_0)$, we introduce

$$\theta(\mathbf{r})=\theta_0+\sum_{\mathbf{K}\,(\neq 0)}\theta(\mathbf{K})e^{i\mathbf{K}\cdot\mathbf{r}} \tag{6}$$

to finally obtain

$$\mathcal{H}=\Omega\left[-\tfrac{1}{2}v\theta_0^2+\tfrac{1}{4}w\theta_0^4+\tfrac{1}{2}\sum_{\mathbf{K}\,(\neq 0)}(4\mu+3w\theta_0^2-v)\theta(\mathbf{K})\theta(-\mathbf{K})+\tfrac{1}{4}w\sum_{\mathbf{K}_1,\mathbf{K}_2,\mathbf{K}_3(\neq 0)}\theta(\mathbf{K}_1)\theta(\mathbf{K}_2)\theta(\mathbf{K}_3)\theta(-\mathbf{K}_1-\mathbf{K}_2-\mathbf{K}_3)\right]. \tag{7}$$

Equation (7) provides a complete description of the long-wavelength orientational degrees of freedom of the overlayer.

The mean-field theory was developed as follows. We assume that the amplitude of each orientational mode is a Gaussian random variable. Then, the internal energy of the hexagonal overlayer $E(\theta_0)$ is equal to the mean value of the Hamiltonian and is given by

$$E(\theta_0)=\Omega[-\tfrac{1}{2}v\theta_0^2+\tfrac{1}{4}w\theta_0^4+\tfrac{1}{2}(4\mu+3w\theta_0^2-v+\tfrac{3}{2}w\langle\theta^2\rangle)\langle\theta^2\rangle]\ . \tag{8}$$

where $\langle\theta^2\rangle=\sum_{\mathbf{K}\,(\neq 0)}\langle\theta(\mathbf{K})\theta(-\mathbf{K})\rangle$ is the mean-square angular fluctuation about $\theta_0$. Gibb's variational principle states that the correct free energy $(F)$ is greater than or equal to $E(\theta_0)-TS$, where $T$ is the temperature and $S$ is the entropy. Therefore, an optimum value of $\theta_0$ is obtained by minimizing $F$ with respect to $\theta_0$. This amounts to minimizing $E(\theta_0)$ with respect to $\theta_0$, because the entropy is independent of $\theta_0$. In this way, we obtain

$$-v+w\theta_0^2+3w\langle\theta^2\rangle=0 \tag{9}$$

for the rotated phase and $\theta_0=0$ for the aligned phase. We may also calculate

$$\frac{\partial^2\mathcal{H}}{\partial\theta(\mathbf{K})\partial\theta(-\mathbf{K})}=\Omega\left[4\mu+3w\theta_0^2-v+3w\sum_{\mathbf{K}_1\,(\neq 0)}\theta(\mathbf{K}_1)\theta(-\mathbf{K}_1)\right]. \tag{10}$$

Using Eq. (10), self-consistent application of the classical equipartition-of-energy theorem yields

$$\langle\theta(\mathbf{K})\theta(-\mathbf{K})\rangle=k_BT/\langle\partial^2\mathcal{H}/\partial\theta(\mathbf{K})\partial\theta(-\mathbf{K})\rangle=\frac{k_BT}{\Omega(4\mu+3w\theta_0^2-v+3w\langle\theta^2\rangle)}=\frac{k_BT}{\Omega(4\mu+2w\theta_0^2)}\ , \tag{11}$$

for the amplitude of orientational fluctuations in the rotated phase. The last equality in Eq. (11) is obtained by employing Eq. (9). Because $\mu$ is a constant, Eq. (11) shows that orientational fluctuations are of finite amplitude for all temperatures ($T < T_c$) and all wave vectors. Therefore, the approximation that the amplitude of each mode follows a Gaussian distribution is expected to be accurate. In contrast, at an ordinary continuous-phase transformation the amplitude of the order-parameter fluctuations diverges as the wave vector of the mode goes to zero. As a result, the amplitude of the fluctuations does not follow a Gaussian distribution and there are important corrections to the mean-field results. In the case of a rotational transformation, the mean-square angular fluctuation about $\theta_0$ is given by

$$\langle \theta^2 \rangle = \frac{N k_B T}{\Omega(4\mu + 2w\theta_0^2)} = \frac{\Lambda^2 k_B T}{4\pi(4\mu + 2w\theta_0^2)} , \tag{12}$$

where $N$ is the total number of orientational modes and $\Lambda$ is the Debye wave vector. (This may be compared to Eq. 4.1 *et seq.* of Ref. 49.) Equation (9) then can be rewritten:

$$-v + w\theta_0^2 + \frac{3\Lambda^2 w k_B T}{4\pi(4\mu + 2w\theta_0^2)} = 0 . \tag{13}$$

At a continuous phase transformation, $\theta_0$ goes to zero at $T_c$. Therefore, $T_c$ may be defined by

$$-v + 3\Lambda^2 w k_B T_c / 16\pi\mu = 0 ,$$

and Eq. (13) becomes

$$w\theta_0^2 + \frac{3\Lambda^2 w}{4\pi}\left[\frac{k_B T}{4\mu + 2w\theta_0^2} - \frac{k_B T_c}{4\mu}\right] = 0 . \tag{14}$$

Near $T_c$, $\theta_0$ is small so that we may make the approximation that

$$\theta_0^2[1 - 3\Lambda^2 w k_B T_c/(32\pi\mu^2)] = 3\Lambda^2 k_B (T_c - T)/(16\pi\mu) . \tag{15}$$

If $3\Lambda^3 w k_B T_c/(32\pi\mu^2) < 1$, there is a continuous phase transformation with

$$\theta_0 = \left[\frac{v}{w[1 - 3\Lambda^2 w k_B T_c/(32\pi\mu^2)]}\right]^{1/2} \times [(T_c - T)/T_c]^{1/2} . \tag{16}$$

The one-half-power-law dependence of the rotation angle on reduced temperature is as expected for a mean-field theory, and is consistent with our observations for the hexagonally reconstructed Pt(001) surface near $T_c$. For

$$3\Lambda^2 w k_B T_c/(32\pi\mu^2) > 1 ,$$

it is straightforward to show that there is a discontinuous change of the rotation angle with temperature (first-order transformation). Such behavior is reminiscent of the rotational transformation of the hexagonally reconstructed Au(001) surface which is primarily discontinuous (Ref. 22 and Sec. IV), in contrast to the mainly continuous transformation of the hexagonally reconstructed Pt(001) surface (Sec. III). However, even at temperatures immediately below the rotational transformation of the Au(001) surface, there is coexistence among domains with differing rotation angles, suggesting the existence of multiple minima in the angle dependence of the interfacial energy. This possibility is not described by Eq. (5), nor is the coexistence of domains with different rotation angles for the Pt(001) surface at temperatures below 1580 K.

For overlayers with an interfacial Hamiltonian that can be approximated by Eq. (5), we expect that mean-field theory should apply. In particular, it may apply to the rare gases on graphite. In this regard, we note that, while the behavior of Ar[2,6] and Kr[4] on graphite is quantitatively predicted by the calculations of Novaco and McTague[1] and of Shiba,[25] the rotational behavior of Xe[5,6] on graphite cannot be understood on this basis. Specifically, in the study of Hong *et al.*[5] it was found that the Xe overlayer showed a discontinuous rotational transformation from a rotated to an aligned phase with increasing incommensurability. The transformation further showed a significant history dependence and, in addition, rotated and unrotated domains were observed in coexistence.[5] In the experiment of D'Amico *et al.*,[6] a continuous decrease of the Xe rotation angle with increasing incommensurability was observed. For Xe on graphite, it is important to note that the incommensurability increases with increasing temperature;[5,6] thus, rotational transformations at which the rotation angle increases continuously[6] or discontinuously[5] with decreasing temperature have already been observed for Xe on graphite. Further work is necessary to clarify whether the mean-field theory presented in this section is relevant for this system. Finally, we note that Clark *et al.*[9] found that the orientation $\theta$ of incommensurate Cs intercalated into a graphite host varies as $\theta = A[(T_c - T)/T_c]^{\beta}$, with $\beta = 0.47$, a result which is also consistent with a mean-field description.

## VI. SUMMARY AND CONCLUSIONS

In this paper, we have presented the results of a synchrotron x-ray-diffraction study of the lateral structure of the clean Pt(001) surface between 300 and 1820 K. Throughout this temperature range the surface exhibits a reconstruction in which atoms in the surface layer are arranged on a corrugated, hexagonal lattice, in spite of the planes of square symmetry immediately beneath. For temperatures decreasing from 1820 K, the average hexagonal lattice distorts slightly, expanding along the cubic $[1\bar{1}0]$ direction and contracting along the [110] direction compared to the bulk lattice. Its areal density relative to that of hexagonal (111) planes in the crystal interior is nearly temperature independent and compressed by $\sim 8\%$. The most dramatic evolution occurs for the orientation of the hexagonal overlayer with respect to the cubic substrate. Between 1820 and 1685 K, the (1,0) hexagonal wave vector is aligned with the cubic (1,1,0) wave vector. However, at a critical temperature of 1685 K, the hexagonal overlayer undergoes a transformation into a phase in which there is nonzero rotation angle between these two directions. Between 1685 and $\sim 1590$ K, the relative rotation angle evolves smoothly with tempera-

ture, following a one-half-power dependence on the reduced temperature. At ~1590 K, domains with a second rotation angle appear. With decreasing temperature, domains with both orientations coexist. Their rotation angles are only weakly temperature dependent between 1590 and 300 K. An additional feature of the hexagonal reconstruction is that the extent of translational order decreases with decreasing temperature from many thousands of Angstroms at 1820 K to ~2000 Å at 300 K.

We have also presented measurements of the orientational epitaxy of the hexagonally reconstructed Au(001) surface. We find a predominantly discontinuous rotational transformation at temperatures below which domains with several discrete rotation angles coexist. When temperatures are scaled to the bulk melting temperature, the overall phase behavior of the Au(001) surface is strikingly similar to that of the Pt(001) surface. Furthermore, the rotation angles observed for the Au(001) surface are similar to those of the Pt(001) surface ( ~0.8°).

It seems clear that current theories of orientational epitaxy are inconsistent with our results: First, that a rotational transformation takes place for the hexagonally reconstructed Au(001) and Pt(001) surfaces accompanied by only a very small corresponding change in the overlayer incommensurabilities; second, that the observed low-temperature rotation angles are nearly an order of magnitude smaller than predicted; and third, that hexagonally reconstructed domains with different rotation angles can coexist. We have developed a mean-field theory of rotational transformations, which describes our observation that the rotation angle of the Pt(001) overlayer follows a one-half-power law versus the reduced temperature. We hope that the measurements presented in this paper will lead to renewed theoretical and experimental interest in rotational transformations, and that more sophisticated and detailed calculations of the structure of Au(001) and Pt(001) surfaces may elucidate their rotational phase behavior.

## ACKNOWLEDGMENTS

We thank F. Grey and J. Bohr for communicating their results prior to publication and for useful discussions. We also thank M. Blume, M. Paczuski, S. C. Fain, Jr., A. D. Novaco, and J. P. McTague for useful discussions. We are especially indebted to G. Ownby for his invaluable help throughout these experiments. The work performed at M.I.T. is supported by the Join Services Electronics Program under Contract No. DAAL 03-89-C-0001 and the U. S. National Science Foundation under Grant No. 8806591. The work at Oak Ridge National Laboratory is sponsored by the Division of Materials Sciences, Office of Basic Energy Sciences, U. S. Department of Energy under Contract No. DE-AC05-84OR21400 with Martin Marietta Energy Systems, Inc. The work performed at Brookhaven National Laboratory is supported by the U. S. Department of Energy under Contract No. DE-AC0276CH00016.

## APPENDIX

An important variable to emerge in the present studies is the rate of sample cooling. More specifically, it seems

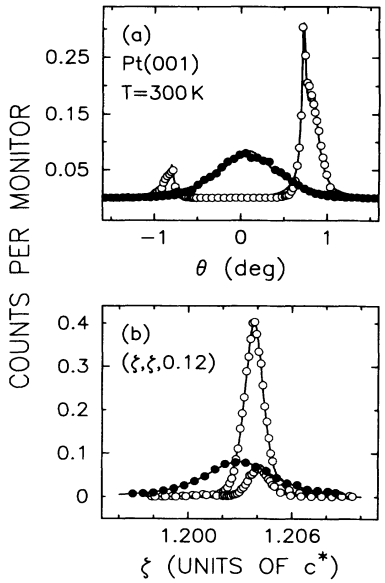


FIG. 19. (a) Angular and (b) radial scans through the (1,0) hexagonal rod of the Pt(001) surface. Open circles correspond to data taken after slow cooling from the disordered phase. Filled circles correspond to data for a quenched state, as described in the text. The two profiles shown as open circles in (b) correspond to radial scans through the two rods, which are shown in (a), one with a positive and the other with a negative sense of rotation.

that rapid decrease in sample temperature can lead to structures which are quantitatively, or even qualitatively, different from those following slow cooling to the same final temperature. While we are unable to prove that the structures produced by slow cooling are at thermal equilibrium, we can illustrate some of the differences which depend on thermal history. Figure 19(a) shows the results of angular scans through the (1,0) hexagonal peak of the Pt(001) surface. The data shown as open circles were collected after slowly cooling the sample from the disordered phase ($T > 1820$ K) to 300 K over a period of

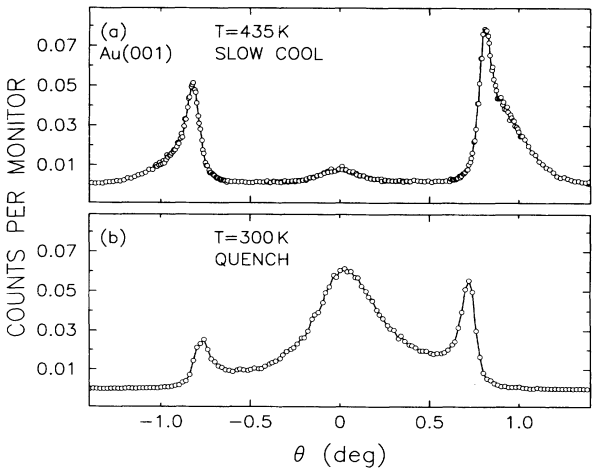


FIG. 20. Angular scans of the (1,0) hexagonal peak of the Au(001) surface obtained after (a) slow cooling and (b) quenching from the disordered phase.

greater than 24 hours, reproducing the profile shown in Fig. 8(h). In contrast, the solid circles in Fig. 19(a) show data which were obtained by first sputtering the surface at 300 K for 30 min (4 $\mu$A, 1 keV), then increasing the temperature rapidly to 1000 K, holding the temperature at 1000 K for 5 min, and finally turning off the sample heater, allowing the sample to cool to 300 K. The angular profile obtained after this procedure shows a single broad peak (0.6° FWHM), which is aligned with the cubic [110] direction (quenched structure). Evidently, a surface prepared in this way shows a hexagonal reconstruction; however, it does not exhibit distinct, nonzero rotation angles. This result is consistent with that of Heinz, Heilmann, and Müller. Figure 19(b) shows the corresponding radial scans through the (1,0) hexagonal peak. Closed circles indicate data collected after rapid cooling. Open circles indicate data collected after slow cooling. It is clear that the radial width of the peak obtained from the quenched structure is three times broader than that obtained from slow cooling, consistent with the presence of smaller ordered domains in the quenched case.

Finally, we illustrate in Fig. 20 that the rate of cooling can have a profound effect on the angular profiles observed for the Au(001) surface. Figure 20(a) reproduces the data shown in Fig. 15(h) and was obtained by slowly cooling the sample from 1200 to 435 K over a period of 24 h. In contrast, the profile of Fig. 20(b) was obtained by rapidly quenching the sample from the disordered phase. The sample temperature, in this case, decreased through the transformation to the aligned-hexagonal phase and through the rotational transformation in only a few minutes. Below $\sim$800 K the cooling rate was slower, but the sample temperature reached 300 K within a few hours. For the quenched sample, the unrotated component of the angular profile appears both more intense and broader than for the slowly-cooled sample. In addition, there are no "0.9°-rotated" domains for the quenched sample. In all cases, it seems that the most ordered surfaces (narrowest radial and angular widths) result from slow cooling.

---

*Present address: European Synchrotron Radiation Facility, Grenoble, France.

[1]A. D. Novaco and J. P. McTague, Phys. Rev. Lett. **38**, 1286 (1977); J. P. McTague, and A. D. Novaco, Phys. Rev. B **19**, 5299 (1979).

[2]C. G. Shaw, S. C. Fain, Jr., and M. D. Chinn, Phys. Rev. Lett. **41**, 955 (1978); S. C. Fain, Jr., M. D. Chinn, and R. D. Diehl, Phys. Rev. B **21**, 4170 (1980).

[3]S. Calisti, J. Suzanne, and J. A. Venables, Surf. Sci. **115**, 455 (1982).

[4]K. L. D'Amico, D. E. Moncton, E. D. Specht, R. J. Birgeneau, S. E. Nagler, and P. M. Horn, Phys. Rev. Lett. **53**, 2250 (1984); E. D. Specht, A. Mak, C. Peters, M. Sutton, R. J. Birgeneau, K. L. D'Amico, D. E. Moncton, S. E. Nagler, and P. M. Horn, Z. Phys. B **69**, 347 (1987).

[5]H. Hong, C. J. Peters, A. Mak, R. J. Birgeneau, P. M. Horn, and H. Suematsu, Phys. Rev. B **36**, 7311 (1987); **40**, 4797 (1989).

[6]K. L. D'Amico, J. Bohr, D. E. Moncton, and D. Gibbs, Phys. Rev. B **41**, 4368 (1990).

[7]T. Aruga, H. Tochihara, and Y. Murata, Phys. Rev. Lett. **52**, 1794 (1984).

[8]D. L. Doering and S. Semancik, Phys. Rev. Lett. **53**, 66 (1984).

[9]R. Clarke, N. Caswell, S. A. Solin, and P. M. Horn, Phys. Rev. Lett. **43**, 2018 (1979).

[10]M. Mori, S. C. Moss, Y. M. Yan, and H. Zabel, Phys. Rev. B **25**, 1287 (1982).

[11]M. G. Samant, M. F. Toney, G. L. Borges, L. Blum, and O. M. Melroy, J. Phys. Chem. **92**, 220 (1988).

[12]H. Li and B. P. Tonner, Surf. Sci. **193**, 10 (1988).

[13]F. Grey, M. Nielsen, R. Feidenhans'l, J. Bohr, J. Skov Petersen, J. B. Bilde-Sørenson, R. L. Johnson, H. Weitering, and T. Hibma (unpublished).

[14]B. M. Ocko, J. Wang, A. Davenport, and H. Isaacs, Phys. Rev. Lett. **64**, 1466 (1990).

[15]S. Hagstrom, H. B. Lyon, and G. A. Somorjai, Phys. Rev. Lett. **15**, 491 (1965); H. B. Lyon and G. A. Somorjai, J. Chem. Phys. **46**, 2539 (1967).

[16]P. W. Palmberg, in *The Structure and Chemistry of Solid Surfaces*, edited by G. A. Somorjai (Wiley, New York, 1969), p. 29-1.

[17]H. P. Bonzel, C. R. Helms, and S. Kelemen, Phys. Rev. Lett. **35**, 1237 (1975).

[18]P. R. Norton, J. A. Davies, D. P. Jackson, and N. Matsunami, Surf. Sci. **85**, 269 (1979).

[19]K. Heinz, P. Heilmann, and K. Müller, Z. Naturforsch. Teil A **32**, 28 (1977); P. Heilmann, K. Heinz, and K. Müller, Surf. Sci. **83**, 487 (1979).

[20]M. A. van Hove, R. J. Koestner, P. C. Stair, J. P. Biberian, L. L. Kesmodel, I. Bartos, and G. A. Somorjai, Surf. Sci. **103**, 189 (1981); **103**, 218 (1981).

[21]R. J. Behm, W. Hösler, E. Ritter, and G. Binnig, Phys. Rev. Lett. **56**, 228 (1986); W. Hösler, E. Ritter, and R. J. Behm, Ber. Bunsenges. Phys. Chem. **90**, 205 (1986).

[22]S. G. J. Mochrie, D. M. Zehner, B. M. Ocko, and D. Gibbs, Phys. Rev. Lett. **64**, 2925 (1990); D. Gibbs, B. M. Ocko, D. M. Zehner, and S. G. J. Mochrie, Phys. Rev. B **42**, 7330 (1990); B. M. Ocko, D. Gibbs, K. G. Huang, D. M. Zehner, and S. G. J. Mochrie, *ibid.* **44**, 6429 (1991).

[23]D. Gibbs, G. Grübel, D. M. Zehner, D. L. Abernathy, and S. G. J. Mochrie, Phys. Rev. Lett. **67**, 3117 (1991).

[24]G. Grübel, D. Gibbs, D. M. Zehner, D. L. Abernathy, and S. G. J. Mochrie (unpublished).

[25]H. Shiba, J. Phys. Soc. Jpn. **46**, 1852 (1979); **48**, 211 (1980).

[26]J. Villain, Phys. Rev. Lett. **41**, 36 (1978).

[27]See, for example, F. Ercolessi, E. Tosatti, and M. Parinello, Phys. Rev. Lett. **57**, 719 (1986); K. W. Jacobsen, and J. K. Nørskov; *ibid.* **60**, 2496 (1988).

[28]K. G. Huang, D. Gibbs, D. M. Zehner, A. R. Sandy, and S. G. J. Mochrie Phys. Rev. Lett. **65**, 3313 (1990); A. R. Sandy, S. G. J. Mochrie, D. M. Zehner, K. G. Huang, and D. Gibbs, Phys. Rev. B **43**, 4667 (1991).

[29]R. J. Needs, Phys. Rev. Lett. **58**, 53 (1987).

[30]R. J. Needs and M. Mansfield, J. Phys. Condens. Matter **1**, 7555 (1989).

[31]B. W. Dodson, Phys. Rev. Lett. **60**, 2288 (1988).

[32]N. Takeuchi, C. T. Chan, and K. M. Ho, Phys. Rev. Lett. **63**, 1273 (1989).

[33]O. Alerhand, D. Vanderbilt, R. D. Meade, and J. D. Joannopolis, Phys. Rev. Lett. **61**, 1973 (1988). See also V. I. Marchenko, Zh. Eskp. Teor. Fiz. **81**, 1141 (1981) [Sov. Phys. JETP **54**, 605 (1981)]; T. Garel and S. Donaich, Phys. Rev. B **26**, 325 (1982).

[34]*NSLS User's Manual: Guide to the VUV and X-Ray Beamlines,* edited by N. F. Gmür (Brookhaven National Laboratory, Upton, New York, 1991).

[35]D. Gibbs, B. M. Ocko, D. M. Zehner, and S. G. J. Mochrie, Phys. Rev. B **42**, 7330 (1990).

[36]*Numerical Data and Functional Relationships in Science and* Technology, edited by O. Madelung, Landolt-Börnstein, New Series, Vol. III, Pt. 14a (Springer-Verlag, Berlin, 1988), p. 30.

[37]R. A. Cowley, Acta Crystallogr. Sec. A **43**, 825 (1987). See also R. Pynn, Y. Fujii, and G. Shirane, *ibid.* **39**, 38 (1983).

[38]We relate the deconvolved FWHM of diffraction maxima associated with finite-sized domains to the domain size ($L$) via $L=2\sqrt{4\pi\ln 2}/\mathrm{FWHM}=5.9/\mathrm{FWHM}$; see for example, P. Dutta and S. K. Sinha, Phys. Rev. Lett. **47**, 50 (1981).

[39]M. Nielsen, J. Als-Nielsen, and J. P. McTague, in *Ordering in Two Dimensions,* edited by S. K. Sinha, (North-Holland, New York, 1980), p. 135.

[40]Surface steps are expected to lead to a broadening of substrate rods only if the steps conspire to produce a divergent height-height correlation function. See, for example, S. R. Andrews and R. A. Cowley, J. Phys. C **18**, 6427 (1985).

[41]F. K. Wen, W. E. Packard, and M. B. Webb, Phys. Rev. Lett. **61**, 2469 (1988).

[42]D. Vanderbilt (private communication).

[43]D. D. Chambliss and R. J. Wilson (unpublished).

[44]J. V. Barth, H. Brune, G. Ertl, and R. J. Behm, Phys. Rev. B **42**, 9307 (1990).

[45]F. Grey and J. Bohr (unpublished).

[46]C. R. Fuselier, J. C. Raich, and N. S. Gillis, Surf. Sci. **92**, 667 (1980).

[47]J. Cui and S. C. Fain, Jr., Phys. Rev. B **39**, 8628 (1989).

[48]R. A. Cowley, Phys. Rev. B **13**, 4877 (1976).

[49]D. R. Nelson and B. I. Halperin, Phys. Rev. B **19**, 2457 (1979).